Journal of Geochemical Exploration 252 (2023) 107262

Contents lists available at ScienceDirect

Journal of Geochemical Exploration

journal homepage: www.elsevier.com/locate/gexplo

Geochemistry of thermal springs and associated gases along the Strymon River Valley (Bulgaria and Greece)

Angelo Minissale [a], Orlando Vaselli [a,b,c,*], Peter Marchev [d], Franco Tassi [a,b]

[a] CNR-IGG – Institute of Geosciences and Earth Resources, Via G. La Pira, 4, 50121 Firenze, Italy
[b] Department of Earth Sciences, Via G. La Pira, 4, 50121 Firenze, Italy
[c] INGV, Via Franceschini, 31, 40100 Bologna, Italy
[d] Geological Institute "Strashimir Dimitrov" – Bulgarian Academy of Sciences, Acad. G. Bonchev st. bl.24, 1113 Sofia, Bulgaria

ARTICLE INFO

Keywords:
Fluid geochemistry
Strymon River
Stable isotopes
Geothermometry
Fluid circulation

ABSTRACT

This paper presents and discusses the water and gas geochemistry of a large number of thermal springs occurring along the N-S trending Strymon Valley, from its source, near Sofia (Bulgaria), to the Aegean Sea (Greece). In Bulgaria springs have markedly alkaline *p*H, relatively low Total Dissolved Solids and prevalent Na-HCO_3 to Na-Cl(SO_4) in composition while the associated gas phase is mostly N_2-dominated. When moving to the Greek sector, the thermal springs, Ca(Mg)-HCO_3 to Na-HCO_3, become less alkaline and more saline whereas the associated gas phase is CO_2-dominated. The abrupt geochemical change in the Greek sector is caused by a variation in the thickness and nature of the sediments filling the Strymon Valley, the latter being characterized by a relevant amount of Neogene marine material. Such changes occur south of an important *E*-W lineament named Middle Mesta, south of which marble formations extensively crop out and are likely occurring below the sedimentary succession. The presence of these carbonate sequences embedded in the Neogene sediments is explaining the CO_2-rich gases associated to the Greek springs. Water isotopes indicate a meteoric origin for the studied waters. From a geothermometric point of view, solute (previous studies) and gas (this work) geothermometers suggest that no high enthalpy systems occur in the Bulgaria and northern sector of Greece with estimated temperatures <120 °C. Consequently, these thermal springs can be regarded as tectonically-derived along the many fault systems that border the Strymon Valley. The convective circuits are thus originated from rainfall in the crystalline massifs that border the valley, *i.e.* the Serbo-Macedonian to the west and the Rhodope to the east.

1. Introduction

The occurrence of thermal springs in any geodynamic context suggests the possible presence of shallow hot reservoirs near the surface, potentially ready to be exploited for industrial (*e.g.* paper production), domestic (*e.g.* space heating), social (*e.g.* balneotherapy) and agricultural (*e.g.* greenhouses) purposes (*e.g.* Towler, 2014). Nevertheless, if the presence of high-enthalpy systems at shallow depth (*e.g.* at plate boundaries) is ascertained, production of electricity can also be predictable.

From a genetic point of view it is known that thermal springs are likely occurring: *i*) at the intersections of faults (*e.g.*: Florinsky, 2016 and references therein), *ii*) in places where thermal aquifers are hosted at the top of buried structural highs where the geothermal gradient is found to be the highest (Minissale, 2018 and references therein), and *iii*) at low elevation(s) in a rugged morphology, typical of river valleys descending from active volcanoes (Ingebritsen et al., 2006). Additionally, other parameters, such as lithology and rock permeability (*i.e.* self-sealing; Facca and Tonani, 1967) and topography (Oliver, 1986) can play a relevant role to favor or disfavor their emergence at the surface.

According to Benderev et al. (2016), the hydrothermal region of Bulgaria can be divided into three main hydrogeological types *i.e.*: stratified, fractured and mixed. From the north to the south: *i*) the Low Danubian Artesian area, which includes the Varna Artesian Basin to the east; *ii*) the Intermediate zone and *iii*) the Rila-Rhodope zone. Most thermal waters are used for ludic or therapeutic purposes whereas geothermal power plants were never installed, likely due the presence of low enthalpy systems, as also suggested by the extensive literature on

* Corresponding author at: CNR-IGG – Institute of Geosciences and Earth Resources, Via G. La Pira, 4, 50121 Firenze, Italy.
E-mail addresses: angelo.minissale54@gmail.com (A. Minissale), orlando.vaselli@unifi.it (O. Vaselli), pmarchev@geology.bas.bg (P. Marchev), franco.tassi@unifi.it (F. Tassi).

https://doi.org/10.1016/j.gexplo.2023.107262
Received 1 April 2022; Received in revised form 4 June 2023; Accepted 11 June 2023
Available online 14 June 2023
0375-6742/Published by Elsevier B.V.

this issue since 1930 (*e.g.*. Radev, 1930; Petrov, 1964, 1973; Petrov et al., 1970; Velinov and Bojadgieva, 1981; Hristov, 1993; Hristov et al., 2010; Bojadgieva et al., 2015).

A relevant number of thermal spring discharges characterizes the N-S oriented Strymon River Valley from close to Sofia to the Aegean Sea in a rather complex geological setting (Fig. 1). The Strymon River (SR, hereafter) intercepts, at the southern boundary of Bulgaria and northern Greece, the Intermediate and the Rila-Rhodope hydrothermal zones. Numerous CO_2-rich thermal discharges are also present in Greece. Here, despite the relevant depth reached by several boreholes, drilled for oil exploration fluid temperatures never exceeded those expected in continental thermal regimes (135 °C at 3650 m depth; Mendrinos et al., 2010). According to Pentcheva et al. (1997), thermal springs in the northern Bulgarian sector of SR are dominated by alkaline *p*H values, have alkaline composition [from Na-HCO_3 to Na-$HCO_3(SO_4)$], fluoride-rich and often radioactive while the associated gases are dominated by N_2. By In the Greek sector of SR, the *p*H values become less alkaline, the Na—Cl fraction increases, and CO_2 tends to dominate the gas chemistry (*e.g.* Minissale et al., 1989; Andritsos et al., 2010, 2011; D'Alessandro and Kyriakopoulos, 2013; Arvanitis et al., 2016).

In this paper, original chemical (main and trace elements) and isotopic (oxygen and hydrogen of water, carbon in CO_2 and helium-3) data of the many thermal emissions and associated gases along the SR Valley, collected during two surveys, are presented. The focus of the study is aimed at highlighting relationships and/or differences of the Bulgarian and Greek sectors to investigate: *i*) the geochemistry of both thermal and not thermal fluid emissions, *ii*) the geodynamic, *iii*) the hydrological and *iv*) the structural context, in an area characterized by distinct fault systems and active tectonics, which produced a rough morphology cut by a N-S-oriented regional lineament where the Strymon river opens its way to the Sea (Zagorchev, 1992; Dinter and Royden, 1993; Brun and Sokoutis, 2007; Tranos, 2011; Kounov et al., 2015).

2. Geological, geomorphological and hydrogeological outlines

The Strymon (or Struma) River originates at the foothills of the Vitosha massif, a 2285 m high plutonic-volcanic edifice located near the city of Sofia (Atanasova et al., 2004; Atanasova-Vladimirova et al., 2010). It flows SW of Sofia and, near the town of Kostendil, it bends S-SE and enters the Aegean Sea in Greece at the Strymon Gulf after about 400 km from the source (Fig. 1).

The valley of SR is located in a very complex geodynamic environment and crosscuts two main metamorphic units, the Rhodope Massif to the east and the Serbo-Macedonian Massif to the west (Fig. 1). Based on similarities in metamorphic grade and structural style, the two massifs are often viewed as a single tectonic element (*e.g.* Ricou et al., 1998). The two massifs are characterized by Palaeozoic and pre-Palaeozoic (Burg, 2012; Meinhold et al., 2010) crystalline, predominantly amphibolite facies, formations and arc-related granitoids emplaced from Cadomian to Alpine times (Antic et al., 2015; Burg et al., 1996; Kaiser-Rohrmeier et al., 2004; Turpaud and Reischmann, 2010). However, the two massifs are characterized by different Cenozoic evolution with strong high-grade Alpine overprint of the Rhodopes and lack of such events in the Serbo-Macedonian massif (Georgiev et al., 2010; Kounov et al., 2010, 2012).

Since the Middle Eocene to Miocene the region has been affected by significant extensional tectonics and core complex formation (Bonev et al., 2006; Brun and Sokoutis, 2007; Dinter and Royden, 1993; Krohe and Mposkos, 2001; Kounov et al., 2015). The exhumation of the core complexes was controlled by two detachment faults: i) Kerdilion (Brun and Sokoutis, 2007) and ii) Strymon (Dinter and Royden, 1993). The timing of the exhumation history and extensional tectonics was determined by low-temperature geochronology (Kounov et al., 2015). The Kerdilion detachment was active between 42 Ma and 24 Ma, whereas the Strymon detachment controlled the exhumation between 24 Ma and 12 Ma following the eastern border of the Struma Basin (see Figs. 1 and 3 in Georgiev et al., 2010). The age of 12 Ma coincides with the beginning of a new episode of extension related to normal faults, some of which cut the Strymon detachment (Georgiev et al., 2010; Kounov et al., 2015). Interestingly, the age coincides with the volcanic activity in the SR, close to Bulgarian-Greece border, and represented by the cryptodome of Kozhuh (12.23 Ma, Georgiev et al., 2013) and the dykes and the nearby subvolcanic bodies of Neopetrisi (11.87 ± 0.11 Ma; Eleftheriadis and Staikopoulos, 1997). These dominant NW-SE-oriented normal faults are related to the formation of several grabens along SR, namely Blagoevgrad, Simitli, Sandanski, Drama and Xanti (*e.g.* Zagorchev, 1992, Fig. 1). Tectonic activity in the area seems to continue till present time (*e.g.* Vrablyanski and Milev, 1993; Glavcheva and Matova, 2010) and is responsible of moderate to low seismicity (Mountrakis et al., 2006), including the strongest earthquake $M_s = 7.2$ that occurred on April 4, 1904 near Kresna (*e.g.* Ambraseys, 2001).

An E-W trending structural element, the Middle Mesta Lineament (MML, hereafter), separates the Bulgarian SR from the Greek SR (Fig. 1). By a geological and morphological point of view, MML has a key role in this subdivision (Burchfiel et al., 2003). The Sandanki valley is indeed relatively narrow whereas the Serres graben, likely formed by a strike-slip faulting (*e.g.* Mouslopoulou et al., 2014) has a funnel shape, opens to the Aegean Sea and is much wider (Fig. 1).

Miocene and Pliocene marine, lacustrine and continental sediments fill the graben systems that form the SR valley (Kojumdgieva et al., 1984; Zagorchev, 1992), The total thickness of the Neogene and Pleistocene deposits varies from 1 to 2 km in northern Bulgarian (Sandanski, Simitli and Blagoevgrad basins) while it is up to 3–3.5 km in the Serres graben (*e.g.* Shterev et al., 1995; Zagorchev, 2007).

The river catchment area is about 18,000 km^2 and the climatic conditions are apparently affected by MML. In fact, typical Mediterranean climate and vegetation, with dry summers and rainy winters, dominate in the southern Greek sector, whereas more humid and continental conditions, with cold winters and relatively frequent abundant snow, affect the Bulgarian part. The SR valley is also bounded, to both the east and west, by elevated isolated mountains and/or belts such as Vitosha (2290 m), Rila (2925 m), Pirin (2915 m), Malesevo (1803 m) and Belasica (2019 m). The relatively heavy precipitations at high elevations are topographically drained into the Strymon river that has a permanent regime, with an annual average flow rate of 2.1 m^3/s (Skoulikidis et al., 2009).

From a hydrological point of view, the sedimentary successions have relatively high permeability in the low horizons in both the Bulgarian (Sandansky graben) and Greek (Serres basin) sectors because of the presence of Miocene basal continental conglomerates (Kojumdgieva et al., 1984). Locally, the presence of the upper clay-rich marine layers in the Greek sector reduces the permeability. The basement metamorphic formations in both the Serbo-Macedonian and Rhodope Massifs and the granites, coinciding with the highest elevations in the study area, have relatively low permeability, which is however enhanced in correspondence of faulting areas (Brun and Sokoutis, 2007; Dinter and Royden, 1993; Kounov et al., 2015; Mendrinos et al., 2010). In the Greek sector, south of MML, marble, embedded in the metamorphic formations, extensively crops out (Fig. 1) and is characterized by high secondary permeability.

3. Sampling and analytical methods

In two close-in-time sampling campaigns, carried out in the 2000s, 59 cold and thermal springs, 7 thermal wells, and 29 samples of bubbling and/or dissolved gases, were collected from the SR valley and adjacent areas, including the Sofia graben (Fig. 1). Based on the mean annual temperature of about 20 °C, particularly in the Greek sector, and considering that in summer the outside temperature can occasionally reach 40 °C, the water samples were divided, as follows: *i*) cold, when temperature was <25 °C, *ii*) thermal, between 25 and 50 °C and *iii*) hot when >50 °C.

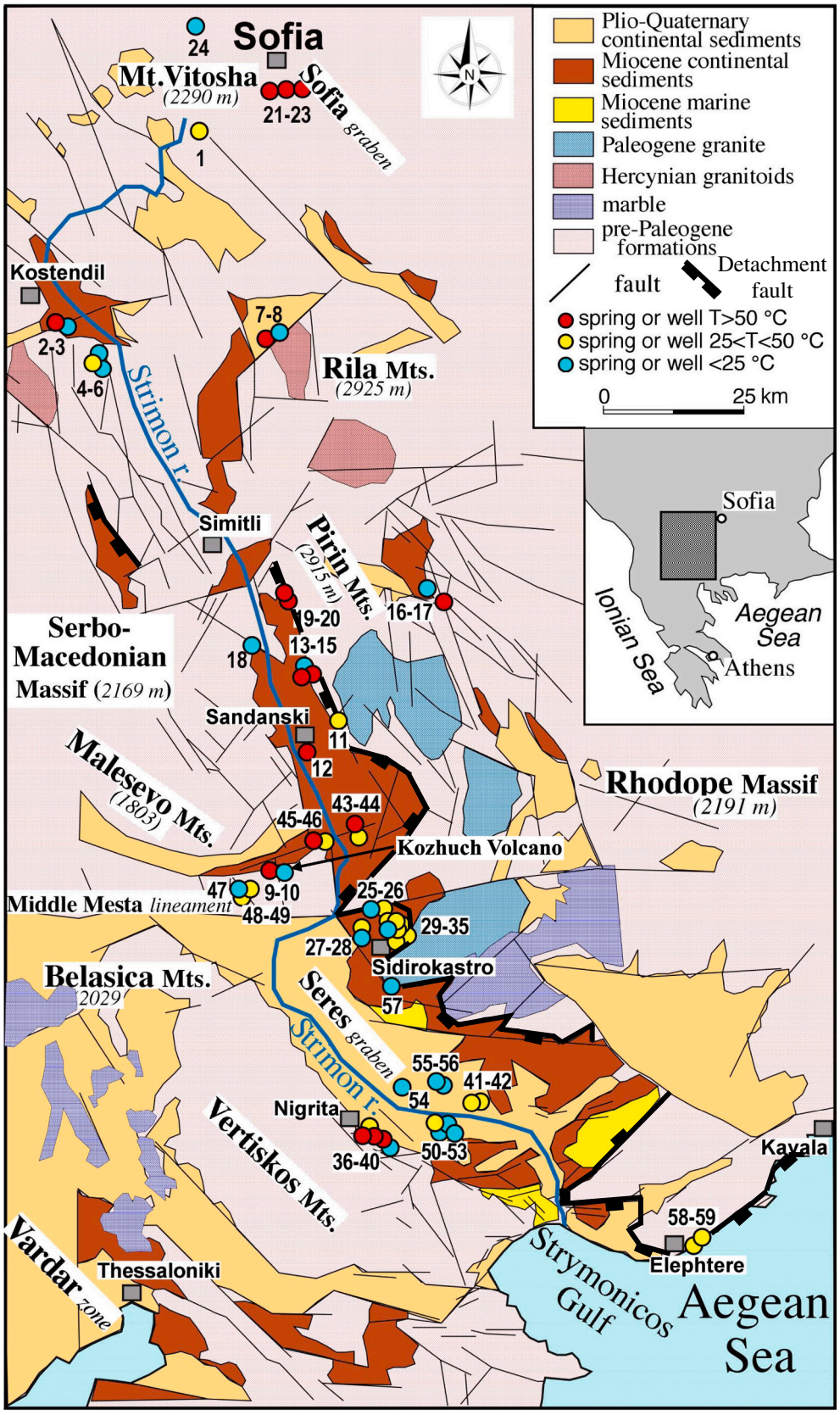

Fig. 1. Geological schematic map of the Strymon River Valley (modified after Shterev et al., 1995) and location of the sampling sites.

Temperature, *p*H, alkalinity (HCO_3 and CO_3^{2-} by acidimetric titration with automatic titration micropipette with 0.01 M HCl and methyl-orange as indicator), SiO_2 and NH_4^+ (by molecular spectrophotometry with Hanna HI93705 and HI93715 portable instrumentations, respectively) were determined in the field.

At each sampling site four aliquots were collected, as follows: *i*) one filtered (0.45 μm) sample for the analysis of F^-, Cl^-, Br^-, NO_3^-, SO_4^{2-}, by ion chromatography with a Dionex DX100 with an analytical error lower than 5 %, and boron by molecular spectrophotometry according to the Azomethine-H method (Bencini, 1985); *ii*) one filtered (0.45 μm) and acidified (suprapur HCl Merck®) sample for the analysis of cations (Na^+, K^+, Mg^{2+}, Ca^{2+} and Li^+), by Atomic Absorption Spectrophotometry with a Perkin-Elmer AAnalyst 100, *iii*) one filtered (0.45 μm) and acidified (suprapur HNO_3 Merck®) sample for the analysis of trace elements (As, Ba, Cd, Cr, Cu, Mn, Mo, Ni, Rb, Se, Sr, W and Zn), carried out by ICP-MS at the Acme Laboratory (Canada), with an analytical error between 10 and 15 % and, finally, *iv*) one unfiltered sample for the isotopic analysis of oxygen and hydrogen (expressed as $\delta^{18}O$ and δ^2H in ‰ *vs.* V-SMOW: Standard Mean Ocean Water) in the water molecule. The analytical results are listed in Table 1 for main and minor components, the $\delta^{18}O$ and δ^2H values and pCO_2 (calculated by using the PHREECQ geochemical code; Parkhurst and Appelo, 1999) while the trace elements in selected samples are reported in Table 2.

The isotopic composition of waters was determined by using standard techniques, *i.e.*: *i*) equilibration of H_2O with CO_2 (Epstein and Mayeda, 1953) for determination of the $^{18}O/^{16}O$ ratio and *ii*) H_2 formation after reaction of water with Zn at 550 °C (*e.g.* Coleman et al., 1982) for $^2H/^1H$; errors were 0.1 and 1.1 ‰, respectively. The $^{13}C/^{12}C$ ratio of carbon in CO_2 (expressed as $\delta^{13}C_{PDB}$ ‰) was determined after extraction and purification of CO_2 from the gas mixture by using the two traps method (liquid N_2 and liquid N_2 + tri-chloro-ethilene, respectively; Evans et al., 1998; Vaselli et al., 2006), with an error of 0.05 ‰. The $\delta^{18}O$, δ^2H and $\delta^{13}C$ were all determined with a Finnigan Delta S mass spectrometer.

The gas phase, where bubbling, was collected by using a funnel positioned upside-down into the water (Giggenbach, 1975) to convoy the gas stream into: *i*) a 60 mL pre-evacuated thorion-tapped vial, pre-filled with 25 mL of a 4 N NaOH solution and *ii*) a 100 mL pre-evacuated thorion-tapped vial for the determination of the $^{13}C/^{12}C$ isotopic ratio in CO_2 (Vaselli et al., 2006). Molecular nitrogen, O_2, Ar, He, Ne, CO, H_2, CH_4 and the $^3He/^4He$ isotopic ratios were measured in the head-space of the NaOH-bearing gas vial. Carbon dioxide and H_2S were measured in the alkaline solution according to Montegrossi et al. (2001) and Vaselli et al. (2006).

The bulk gas composition (main and minor compounds) and CH_4 were determined by gas chromatography, with two Shimadzu (GC-14A and GC-15A) gas chromatographs equipped with thermal conductivity and flame ionization detectors, respectively. Carbon dioxide and H_2S were measured by acidimetric titration and ion chromatography (as SO_4) in the alkaline solution (Montegrossi et al., 2001; Vaselli et al., 2006).

Analytical errors were lower than 3 % for the main gas species and lower than 10 % for the minor components.

Dissolved gases from 14 thermal waters were also collected in pre-evacuated and pre-weighed 250 mL glass flasks also tapped with Teflon stopcocks at equilibrium conditions (STP, Standard Temperature and Pressure; Capasso and Inguaggiato, 1998) where the depressurization favors the water to enter the gas flask filled by 2/3 with deionized water (Tassi et al., 2009). The Shimadzu gas-chromatographers were also used for determining the gas composition in the headspace of the sampling flasks (*e.g.* Vaselli et al., 2006; Tassi et al., 2018). The gas species in the liquid phase were calculated according to the Henry's law constants (Wilhelm et al., 1977). The analytical error for GC analysis was ≤5 %.

The $^3He/^4He$ isotopic ratios of the gas samples, expressed as R/R*a* (where R is the $^3He/^4He$ measured ratio in the sample and R*a* is that of the air: 1.39×10^{-6}), were performed in selected sites. The isotopic ratio was determined according to Magro and Pennisi (1991), by using a Map 215–50 magnetic mass spectrometer, equipped with an ionic-counting device. Resolution was close to 600 amu (=$1.66{\cdot}10^{-27}$ kg) for HD-^{3}He at 5 % of the peak. Analytical error was estimated to be <5 %. The $^3He/^4He$ ratios were corrected for air contamination using the He/Ne ratio (Craig et al., 1978), according to the following equation:

$$R/Ra = ((R_m/R_a)x - 1)/(x - 1)$$

where R_m is the measured $^3He/^4He$ ratio of the sample and *x* is: $(He/Ne)_{sample}/(He/Ne)_{air}$. All chemical and isotopic gas data are reported in Table 3.

4. Results

4.1. Water chemistry

Most emergences were from natural springs, either cold or hot, and a few samples were collected from shallow wells, generally drilled by local Spas, near natural manifestations. Locality and type of emission are listed in Table 1. The *p*H values were highly variable from 6.07 to 9.34, as well as salinity (TDS = Total Dissolved Solids) from 75 up to 4568 mg/L. In most cases, the samples with highest TDS values are characterized by the lowest pH values. This is the case for the waters discharging within the southern Greek part of the SR Valley. On the other side, most high temperature waters have relatively low TDS (<1000 mg/L; *e.g.* #7, #43) that, in the great majority, are related to the northern Bulgarian sector of SR.

The studied waters are plotted in the square diagram (Fig. 2) by Langelier and Ludwig (1942) and belong to three different geochemical facies: *i*) Ca(Mg)-HCO_3, mostly represented by cold waters from Bulgaria; *ii*) Na-HCO_3, characterizing those waters discharging from both sectors and *iii*) Na-Cl(SO_4), both thermal and hot waters as well as a few cold waters, all located in the Bulgarian area, with the exception of #58.

To better discriminate the chemical composition of the SR valley waters and emphasize their marked alkalinity, the water samples were plotted in the salinity (in mg/L) *vs.* (HCO_3 + CO_3 + Na + K) binary diagram of Fig. 3. The most saline samples (>1000 m g/L), independently by the temperature, show a Na(K)-HCO_3 composition with (HCO_3 + Na + K) always >50 % and up to >90 % of total salinity. Apart from sample #1 near Sofia, these water types are mostly located in Greece or along the MML (#9–10, #25–35, #41–42, #58–459). Among the springs with salinity <1000 mg/L, three hot (>50 °C) samples, (# 2, #7, #19–20) and some cold and thermal springs (# 5, 6, 18) discharging in the Bulgarian sector, are dominated by a rather uncommon Na-Cl (SO_4) composition, apparently in contrast with the marked alkalinity of their *p*H values (Table 1). To explain the difference in salinity and *p*H, and, indirectly, the different main composition of springs between the Bulgarian and the Greek sectors, the presence of CO_2-rich bubbling gases or high pCO_2 waters in the Greek sector has to be considered. In fact, CO_2 increases the acidity of the circulating waters at depth and, at the same time, enhances the solution aggressiveness and the alteration strength on silicate and carbonate minerals.

As far as the minor dissolved compounds are concerned, setting aside the two cold waters #10 and #47 that had high concentrations of nitrates (34 and 230 mg/L, respectively), although the remaining SR waters showed contents <11 mg/L. The concentration of fluoride was relatively high in most samples related to the Bulgarian side (up to 17 mg/L) whereas in the Greek sector they were <4.5 mg/L. Bromide contents were <0.8 mg/L with the exception of two samples discharging close to the northern coastal area of the Aegean Sea (#58 and #59) that also showed boron concentrations up to 2.48 mg/L, although the highest abundance of boron pertained to #37 (6.4 mg/L). Lithium was varying from 0.01 to 1.90 mg/L, the highest content being measured in #24 that

Table 1
Chemical (major and minor components) and isotopic composition of water samples from the Strymon Valley. All species, including salinity (TDS = total dissolved solids), are in mg/L; $\delta^{18}O$ and δD in ‰ *vs.* SMOW.

No	Sample	Type	T (°C)	*p*H	TDS	pCO_2	Ca	Mg	Na	K	HCO_3	CO_3	SO_4	Cl	SiO_2	Li	B	NO_3	Br	NH_4	F	$\delta^{18}O$	δ^2H
1	Biala Voda	ts	27.0	6.92	2542	−0.83	18	8.6	690	11	1324	–	400	65	20	0.35	0.73	0.2	0.30	0.54	3.1	−11.11	−77.9
2	Kiustendil	ts	73.0	8.89	602	−3.45	1.5	0.34	153	6.6	153	11	150	31	77	0.18	0.65	0.1	0.10	8.3	10	−11.39	−85.5
3	Nevestino	cs	16.0	7.68	662	−2.23	57	22	67	4.7	339	–	114	16	38	0.06	2.90	0.3	0.20	0.45	1.0	−10.13	−68.2
4	Slatino XG	ts	26.0	9.34	753	−4.49	2.7	0.065	221	3.9	62	13	286	120	23	0.15	2.60	0.3	0.30	2.1	17	−10.37	−77.3
5	Slatino 2	cs	22.5	9.24	846	−4.35	3.3	0.075	262	3.5	78	13	290	110	68	0.12	2.70	0.2	0.40	2.0	14		
6	Slatino GI	cs	20.5	9.33	786	−4.39	2.7	0.028	252	1.6	75	14	284	118	23	0.12	0.68	0.4	0.50	1.5	12		
7	Sapareva XG	tsg	96.5	8.68	839	−3.16	4.6	0.24	180	8.6	170	9	223	36	185	0.15	0.58	0.4	0.20	3.6	17	−11.40	−83.5
8	Sapareva German bridge	cs	9.0	8.54	75	−4.04	8.0	2.0	3.2	1.2	25	4	10	1.8	15	<0.01	3.40	1.5	<0.01	0.02	<0.1	−11.05	−73.3
9	Kozhuch	tsg	73.0	6.69	2147	−0.26	17	11	508	38	1348	–	115	23	81	0.42	0.13	0.3	0.20	0.10	5.2	−10.34	−69.9
10	Kozhuch cold	cs	12.5	7.47	803	−2.04	105	35	53	2.0	342	–	160	38	34	<0.01	0.30	34	0.20	0.10	<0.1		
11	Spatovo north well	tw	33.4	8.97	515	−3.76	4.7	0.38	141	0.8	129	11	178	15	23	0.02	0.11	0.6	0.10	0.44	11	−11.39	−76.3
12	Sandanski	ts	73.0	7.94	632	−2.21	7.2	0.39	132	2.7	262	–	103	10	98	0.10	0.14	0.3	<0.01	<0.01	7.1	−10.85	−70.9
13	Gradeschniza 1	ts	70.0	8.52	506	−2.99	3.9	0.32	110	3.9	167	8	95	14	91	0.17	0.13	0.2	0.10	<0.01	13	−11.73	−74.6
14	Gradeschniza 2	ts	57.5	8.51	503	−3.01	3.8	0.38	121	3.5	185	8	105	9.0	55	0.18	0.02	0.4	0.10	0.10	12		
15	Gradeschniza fountain	cs	10.0	8.53	131	−3.64	27	1.87	2.1	0.8	75	6	5.6	0.2	12	<0.01	0.35	0.8	<0.01	<0.01	<0.1	−8.93	−63.5
16	Dolmo Osenovo	tsg	58.0	8.73	524	−3.50	5.3	0.55	124	3.9	120	9	158	11	84	0.23	0.11	0.4	0.10	0.48	8.6	−11.24	−79.1
17	Dolmo Osenovo cold	cs	13.0	7.84	544	−2.42	48	18	52	1.2	320	–	74	1.0	26	0.12	0.14	0.5	<0.01	<0.01	1.9		
18	Krupich well 3	cw	13.0	9.05	319	−4.10	3.7	0.33	85	1.2	78	10	95	18	21	0.19	0.29	0.3	0.20	0.08	4.6	−10.23	−69.5
19	Dolmo Banja spring	ts	54.0	8.74	594	−3.44	9.7	0.35	170	3.1	88	8	258	10	34	0.23	0.35	0.09	0.05	0.08	13		
20	Dolmo Banja well	tw	70.0	8.80	565	−3.70	9.2	0.29	145	3.1	70	8	249	14	53	0.23	0.74	0.1	0.50	<0.01	13		
21	Kasicene 1R	tsg	75.5	6.64	753	−0.72	53	9.4	106	12	390	–	110	6.0	62	0.13	0.62	0.1	0.10	0.48	2.6		
22	Radmo Pole	ts	58.0	6.78	748	−0.92	42	11	114	12	445	–	65	5.0	50	0.15	0.77	0.5	<0.01	0.79	1.8		
23	Radmo Pole 2	ts	50.5	6.88	755	−1.08	46	11	114	12	439	–	79	6.0	45	0.12	0.70	0.3	0.10	0.91	1.6		
24	Novi Iskar	tsg	24.0	7.33	4568	−0.93	14	14	1185	22	2922	–	352	31	22	1.90	0.77	0.5	0.20	0.13	2.4		
25	Aghistro 1	cs	17.2	7.39	351	−2.11	48	5.8	24	1.2	214	–	30	5.5	19	0.01	0.53	2.8	0.02	0.02	1.0		
26	Aghistro 2 thermal bath	tsg	39.0	7.79	418	−2.45	37	4.4	56	3.1	183	–	71	6.5	54	0.11	0.47	1.0	0.05	<0.01	1.4	−10.03	−66.8
27	Aghistro 3	cs	16.8	7.68	314	−2.41	56	6.9	3.5	0.8	215	–	10	6.0	13	0.01	0.38	2.5	0.02	0.07	0.15		
28	Sidirokastro thermal bath	ts	43.8	6.48	1595	−0.48	120	21	243	36	827	–	192	41	105	0.56	2.74	4.0	0.10	0.06	3.5		
29	Sidirokastro 2	ts	33.9	6.79	1657	−0.84	117	22	263	40	854	–	210	40	102	0.60	2.82	0.5	0.10	0.20	4.8		
30	Sidirokastro 3	ts	30.9	7.92	134	−3.00	16	1.9	7.6	1.2	71	–	8.9	1.9	24	<0.01	0.35	0.3	0.01	<0.01	0.09		
31	Sidirokastro 4	tsg	44.3	6.21	1834	−0.09	70	24	324	43	1069	–	195	33	68	0.47	2.65	0.3	0.20	0.23	4.0	−9.64	−66.9
32	Sidirokastro 5 (SD-5)	tw	41.9	6.54	1890	−0.42	63	27	357	37	1129	–	200	25	45	0.41	2.65	0.2	0.10	0.31	3.0		
33	Termopigi	cs	25.9	7.35	600	−1.84	78	7.5	57	1.6	339	–	47	20	28	0.04	0.35	21	0.05	0.07	0.5		
34	Termopigi-Olmo	ts	34.1	6.68	1346	−0.79	43	20	246	37	720	–	135	35	100	0.55	2.56	2.1	0.20	0.03	4.5		
35	Sidirokastro pool	cs	24.0	7.19	597	−1.64	93	9.8	26	3.5	381	–	37	12	26	0.04	0.49	9.0	0.10	0.18	0.4		
36	Therma-Nigrita	tsg	48.0	6.41	2627	−0.12	77	75	479	55	1678	–	109	40	107	0.77	1.96	0.5	0.30	0.35	2.5		
37	Therma 1-Nigrita	tsg	60.0	6.68	3653	−0.14	65	88	663	98	2318	–	150	165	95	1.20	6.40	0.3	0.80	0.42	2.5	−8.74	−62.5
38	Therma (TH-10)-Nigrita	twg	58.5	6.74	3476	−0.21	79	92	615	93	2318	–	128	55	88	1.07	3.25	0.3	0.70	0.46	1.3		
39	Therma well-Nigrita	cw	17.1	7.37	1354	−1.52	69	60	180	25	854	–	69	41	44	0.30	1.13	11	0.25	0.13	0.6		
40	Therma O-2TS-Nigrita	tsg	50.0	6.65	3841	−0.22	140	110	638	93	2471	–	150	120	108	1.18	7.20	0.6	0.80	0.73	1.4	−8.84	−61.4
41	Ivira (29)	tw	25.3	8.31	774	−2.66	12	9.0	188	2.7	441	10	49	26	35	0.04	0.46	0.1	0.17	0.85	0.3		
42	Ivira (30)	tw	28.2	8.68	1441	−2.71	0.75	1.5	375	1.6	952	19	23	27	37	0.04	0.94	0.5	0.30	1.37	1.5	−9.98	−69.7
43	Levunovo	tsg	83.5	7.34	908	−1.37	10	0.5	204	7.4	381	–	165	23	109	0.30	0.66	0.5	0.15	<0.01	6.5	−9.65	−70.9
44	Levunovo 1	ts	35.5	8.12	906	−2.49	9.6	3	222	3.5	397	–	200	11	49	0.14	0.57	0.2	0.10	0.17	11		
45	Marikostinovo	tsg	39.1	8.12	1089	−2.41	23	4.5	243	9.0	458	–	240	22	81	0.29	0.61	0.4	0.10	<0.01	8.5		
46	Marikostinovo 1	ts	55.0	7.60	980	−1.82	21	4.5	240	8.6	398	–	215	26	57	0.28	0.60	0.8	0.10	0.05	8.0	−11.02	−71.3
47	Petric	cs	19.8	7.16	1196	−1.57	160	56	55	7.4	458	–	134	61	34	0.03	0.38	230	0.60	0.25	0.4		
48	Hotovo	ts	37.8	9.22	509	−3.96	4.1	0.2	131	1.2	151	16	145	17	37	0.01	0.47	0.2	0.12	0.41	6.0	−11.31	−78.2

(*continued on next page*)

Table 1 (*continued*)

No	Sample	Type	T (°C)	*p*H	TDS	pCO_2	Ca	Mg	Na	K	HCO_3	CO_3	SO_4	Cl	SiO_2	Li	B	NO_3	Br	NH_4	F	$\delta^{18}O$	δ^2H
49	South Petric Viss Dol	ts	30.6	7.58	1606	−1.59	9.7	6	408	12	976	–	95	37	54	0.13	1.71	0.3	0.20	0.28	6.5		
50	Lithotopos LI-1	tw	39.2	7.45	1499	−1.47	19	10	370	15	824	–	160	45	51	0.26	1.71	0.2	0.20	0.34	3.0	−9.65	−65.3
51	Lithotopos	cs	16.8	7.77	304	−2.57	44	9.0	11	2	183	–	17	11	27	<0.01	0.35	0.3	0.05	0.11	0.3		
52	Lithotopos lake	cs	18.9	7.15	554	−1.61	42	28	36	3.9	390	–	0.06	8.0	39	<0.01	0.42	0.2	0.05	5.3	0.3		
53	Skoutari	ts	21.5	7.86	462	−2.46	44	13	55	2.0	275	–	29	14	30	0.01	0.51	0.05	0.10	0.10	0.3	−10.16	−69.1
54	Vambakussa	ts	25.0	8.12	533	−2.62	27	8.4	83	2.0	336	–	28	7.5	41	0.01	0.58	0.2	0.05	0.11	0.6		
55	S.Eleni	cs	18.5	7.59	582	−2.05	42	13	77	2.7	397	–	0	15	34	0.01	0.45	0.3	0.15	0.46	0.3		
56	S.Eleni 1	ts	22.2	7.70	625	−2.13	28	11	107	2.3	398	–	34	7.5	36	0.02	0.65	0.02	0.04	<0.01	0.5	−9.54	−63.7
57	Skoutari 1	cs	18.0	7.77	454	−2.38	22	3.5	96	0.8	278	–	6.5	18	29	<0.01	0.46	0.25	0.10	0.15	0.4		
58	Elephtere	tsg	39.0	6.09	2408	0.06	86	17	600	49	915	–	91	590	52	1.01	2.20	0.2	2.30	0.55	1.4		
59	Elephtere 1	tsg	41.2	6.07	2952	0.09	151	17	680	54	1281	–	94	620	46	1.12	2.48	0.2	2.50	0.86	1.4	−7.52	−48.0

ts = thermal spring; tsg = thermal spring with gas; tw = thermal well; twg = thermal well with gas; cs = cold spring; cw = cold well.

also has the highest TDS (4658 mg/L). Ammonia concentrations were up to 8.30 mg/L (#2). Finally, silica (as SiO_2) contents were included in a relatively wide concentration range (from 11.5 to 185 mg/L), the highest contents mostly belonging, as expected, to the >50 °C waters.

The concentrations of selected trace elements (in μg/L) were only determined in the thermal and hot samples (Table 2) and showed a relatively large variability. Cadmium had the lowest contents, never exceeding 1.1 (#13) μg/L while slightly higher values were registered by Cu, Ni and Se (up to 3.8 μg/L: #28, 8.0 μg/L: #22 and 9.8 μg/L: #2, respectively). Molybdenum was varying between 1 (#49) and 36 (#18) μg/L. Chromium and Zn were always below 100 μg/L, although most samples were below 19.4 (#9) and 42.9 (#43), respectively. Manganese showed a remarkable variation. Eight samples had concentrations below the instrumental detection limit (0.1 μg/L) while the highest content of Mn was 154 μg/L (#50). Similarly to manganese, both Ba and W were spanning within a large concentration interval, being comprised between 0.6 (#16) and 169 (#59) and 0.2 (#56) and 165 (#7) μg/L, respectively. Rubidium and Sr contents were also largely variable, their concentrations being between 0.6 (#11 and #56) and 349 (#36) μg/L and 39 (#42) and 1880 (#28) μg/L, respectively. It is noteworthy to point out the arsenic contents were, with exception of 11 samples (# 2–4, 15–16, 28, 42–49), much higher than 10 μg/L and up to 911 (#36) μg/L.

The oxygen and hydrogen isotopes were determined in 25 water samples (Table 1). The most negative values were pertaining to the Bulgarian sector: −11.73 (#13) and −83.5 (#7) ‰ V-SMOW, respectively, whereas the water sample discharging close to the Aegean Sea (#59) was enriched in heavier isotopes with $\delta^{18}O$ and δD values of −7.52 and −48.0 ‰ V-SMOW, respectively.

4.2. Gas geochemistry and isotopic composition

The gas composition of the SR gases (both free and dissolved) can be conveniently described by using multiple diagrams (Fig. 4) that include: N_2 *vs.* CO_2 (top left) and *vs.* Ar (bottom left), and Ne *vs.* Ar (top right) and *vs.* N_2 (bottom right). The N_2—Ar, Ne—Ar and Ne—N_2 diagrams, other than the investigated samples, include: *i*) as a star the composition of air (N_2 = 78 % and Ar = 0.9 %) and, as dashed lines: *ii*) the dilution line with air (where the N_2/Ar ratio is about 83), *iii*) the dilution line with an atmospheric component deriving from Air Saturated Water (ASW at 20 °C where the N_2/Ar ratio is about 39; Giggenbach, 1991). The Ne—Ar diagram also reports the mixing line of ASW at 70 °C, along which several samples lined up.

The two main components, *i.e.* N_2 and CO_2, plotted in Fig. 4a, suggest the presence of two different groups: *i*) high CO_2 (>90 %) and relatively low N_2 (#9, #30, #36–38, #40, #58 and #59) at the right bottom corner and *ii*) high N_2 (>60 %) and low CO_2 (<30 %), with variable quantities of CH_4 (up to 36 % in #51) on the left side. Only one sample (#45) was marked by CH_4 > 60 % and $N_2 \approx 30$ %.

In the N_2—Ar diagram (Fig. 4b), the gas samples characterized by N_2 and Ar concentrations higher than that of the Air (>78 and 0.93 % by vol., respectively, *e.g.* #2, #3, #7, #11, #13, #16, #20) likely imply an indirect enrichment of the less soluble gases whereas O_2 is consumed by typical oxidative processes underground, without the input of extra-atmospheric components. In the N_2—Ar and N_2—Ne (Fig. 4c) plots, it is also visible that samples #9, #37 and #59 have some N_2-excess of not atmospheric origin. The Ne—Ar plot (Fig. 4d) suggests that, in all samples, independently from the main component (either N_2- or CO_2-dominated), the two species have atmospheric ratios that seem to derive from exsolution of ASW at 70 °C. This temperature, which incidentally coincides with the emergence temperature of samples #9 and #37 seems to be also the original deep temperature of several other samples (#40, #59, #45…*etc.*), possibly cooled by conduction or mixing with shallow aquifers of the associated waters as they rise up to the surface.

To investigate the origin of the gas phase in the more representative sites along the SR, eleven and twelve samples were analyzed for $^{13}C/^{12}C$

Table 2
Concentration (in μg/L) of selected trace elements from the SR valley waters.

N°	Sample	Type	Temp.	pH	Cr	Mn	Ni	Cu	Zn	As	Se	Rb	Sr	Mo	Cd	Ba	W
1	Biala Voda	ts	27.0	6.92	15.6	<0.1	3.2	0.5	1.5	105.0	4.0	39.3	1440	12	0.20	19.6	16.0
2	Kiustendil	ts	73.0	8.89	0.7	<0.1	<0.1	0.2	2.1	4.8	9.8	54.8	140	10	0.07	0.7	111.0
4	Slatino XG	ts	26.0	9.34	<0.1	<0.1	2.2	0.8	4.2	2.2	4.1	20.2	365	6	0.10	5.4	54.0
7	Sapareva XG	tsg	96.5	8.68	<0.1	0.8	1.9	1.1	6.6	2.7	3.5	80.9	192	10	0.18	1.6	165.0
9	Kozhuch	tsg	73.0	6.69	19.4	<0.1	2.3	0.7	3.2	15.6	3.9	203.0	969	5	0.10	88.5	38.4
11	Spatovo north well	tw	33.4	8.97	0.6	1.6	1.3	0.6	6.6	14.3	2.8	0.6	73	15	0.06	21.1	70.2
12	Sandanski	ts	73.0	7.94	7.4	1.0	2.2	0.7	2.7	21.9	3.8	13.3	147	13	0.19	2.6	42.5
13	Gradeschniza 1	ts	70.0	8.52	0.6	1.2	1.0	0.4	4.8	19.8	3.1	24.0	106	23	1.10	28.3	38.7
16	Dolmo Osenovo	tsg	58.0	8.73	<0.1	<0.1	0.8	0.5	2.0	0.9	2.5	42.7	119	7	0.03	0.6	34.4
20	Dolmo Banja well	tw	70.0	8.80	0.7	2.5	1.7	0.7	12.2	20.1	3.6	24.1	553	15	0.23	18.8	79.9
21	Kasicene 1R	tsg	75.5	6.64	<0.1	22.4	7.8	0.8	6.4	271.0	3.1	56.4	1190	6	0.16	160.0	29.7
22	Radmo Pole	ts	58.0	6.78	<0.1	60.0	8.0	1.0	8.8	266.0	3.8	40.5	1290	7	0.07	118.0	11.7
24	Novi Iskar	tsg	24.0	7.33	82.8	1.6	1.0	1.0	0.8	14.1	<0.1	73.8	102	17	0.39	1.8	2.9
26	Aghistro 2 thermal bath	tsg	39.0	7.79	0.5	0.5	1.2	1.4	11.1	25.8	0.4	23.1	161	8	0.39	7.3	27.0
28	Sidirokastro thermal bath	ts	43.8	6.48	0.3	0.8	2.7	3.8	35.2	2.6	0.8	220.0	1880	4	0.62	62.5	6.0
36	Therma 1-Nigrita	tsg	60.0	6.41	18.8	<0.1	1.5	0.8	4.5	911.0	1.5	459.0	296	3	0.03	21.5	2.0
42	Ivira (30)	tw	28.2	8.68	11.0	1.0	<0.1	0.1	7.4	1.1	0.6	0.9	39	7	0.05	6.7	3.5
43	Levunovo	tsg	83.5	7.34	0.3	38.4	0.9	1.5	42.9	0.8	0.4	59.3	859	4	0.22	97.7	55.4
46	Marikostinovo 1	ts	55.0	7.60	0.3	4.3	1.4	0.9	17.2	2.9	0.3	47.3	1150	4	0.15	55.4	82.4
49	South Petric Viss Dol	ts	30.6	7.58	9.1	0.5	0.7	0.3	2.6	0.7	0.5	35.7	1110	1	0.01	81.4	5.9
50	Lithotopos LI-1	tw	39.2	7.45	0.3	154.0	1.6	1.5	99.2	34.1	0.4	116.0	470	2	0.42	71.4	1.3
56	S.Eleni 1	ts	22.2	7.70	2.5	2.8	0.3	0.3	<0.1	4.6	<0.1	0.6	276	6	0.03	26.3	0.2
59	Elephtere 1	tsg	41.2	6.07	3.9	<0.1	0.5	0.3	0.2	741.0	6.9	349.0	1570	<1	0.02	169.0	1.2

in CO_2 and the $^3He/^4He$ isotopic ratios (Table 3), respectively. The $\delta^{13}C$-CO_2 values were varying from −9.4 (#21) and −0.7 (#37) in $^o/_{oo}$ *vs.* PDB, while those of helium-3 (expressed as Rc/R*a*) were always <1, the highest ratios being measured at #36 (0.74R*a*), #26 (0.61R*a*), #30 (0.58 R*a*), #50 (0.57R*a*) and #43 (0.54 R*a*).

5. Discussion

5.1. Origin of fluids and fluid components

After Craig (1961), the origin of natural waters at the emergence, at least in terms of altitude and latitude of their parent rainfall, can be established by using the relative D/H and $^{18}O/^{16}O$ isotopic ratios (expressed as δD ‰ and $\delta^{18}O$ ‰). In this study, the oxygen and hydrogen isotopes were analyzed in selected sites and they were varying: from −11.7 (#13) and −7.5 (#59) and from −85.5 (#2) and −48.0 (#59), respectively. The likely local meteoric line, as suggested by several aligned cold samples, the Global (Craig, 1961) and the eastern Mediterranean (Gat and Carmi, 1970) water lines are plotted in the δD-$\delta^{18}O$ diagram of Fig. 5. To the best of our knowledge, no isotopic data for natural waters along the SR are available. Consequently, the likely recharge elevations (in m) of the parent rainfall and shown in Fig. 5 was calculated by using a $\delta^{18}O$ vertical gradient of 0.2 δ‰/100 m measured in central and southern Italy (Longinelli and Selmo, 2003; Minissale and Vaselli, 2011), whose meteorological conditions are not strongly differing with respect to those of the study area. Most thermal and cold waters are distributed between the Global and the eastern Mediterranean lines, suggesting a meteoric origin for most of the SR waters. However, a small ^{18}O positive shift for those samples characterized by the highest temperatures (*e.g.* # 2, #7, #43) was evidenced. As previously mentioned, an attempt to reconstruct the local meteoric water line was carried out by using the coldest water samples (*i.e.*: #3, #18, #53, #56), which would allow to more clearly evidence the possible ^{18}O-shift of some of the hot waters, especially from the Bulgarian side (#2, #4, #7) and Nigrita (#37–40) in Greece. If local evaporation is excluded, though possible when the duct before the emergence is not sealed and/or there is an open-air flow before the emergence site, the ^{18}O-shift is <1.0–1.5 δ‰, suggesting, in general, low deep equilibration temperatures at all sites (*e.g.* Clark and Fritz, 1997). Additionally, the computed recharge elevation of the parent rainfall recharge, for both thermal and cold emergences, is relatively high (>1300 m), which seems to be reasonable if the several high peaks (>1500 m), surrounding the SR valley, are considered.

The relative dependence of temperature with *p*H, TDS, SiO_2 and alkalinity, the latter expressed in terms of *p*H values and partial pressure of CO_2 (pCO_2 = -logPco_2) calculated by the PHREEQC geochemical code (Parkhurst and Appelo, 1999) is reported in Fig. 6. The temperature *vs.* *p*H (Fig. 6a) diagram shows that the low temperature waters from both Bulgaria and Greece are characterized by *p*H > 7 values, due to typical water-rock dissolution processes with silicate and carbonate rocks. The quite high *p*H values (up to 9) of the hot waters from Bulgaria (*e.g.* #2, #7, #16), which show relatively low salinity values (see Fig. 6b), can mostly be related to interaction processes with silicate rocks, which are less prone to alteration with respect to the partly *p*H-buffered solutions deriving by the dissolution of carbonate rocks, the latter prevalently dominating the Greek sector. Exceptions are related to: #9 (a hot water discharging near the 12.2 Ma old Kozhuch volcano, the youngest volcanic activity in Bulgaria, #21-#23), where the lower *p*H are due to the presence of a higher concentration of dissolved CO_2 (Table 3), similar to the Greek waters (#31–34, #36, #58, #59), discharging from the southern sector of SRV. The thermal and hot waters #12, #43, #46 are in between the two described groups.

The temperature *vs.* pCO_2 (as log) diagram (Fig. 6c) mimics, due to the intimate relation between the two parameters, that of temperature *vs.* *p*H (Fig. 6a). Nevertheless, it is to be pointed out that most samples lie to the right of water samples at pCO_2 equilibrated with the atmosphere (−3.8) and samples characterized by CO_2-rich free gases, *i.e.* to the left of the line where Pco_2 > 1 atm (pCO_2 > 0). The Kozhuch water sample (#9) in Bulgaria and those from Therma-Nigrita (#36–38, #40) Sidirokastro (#28, #31–32) and Elephtere (#58–59) in the Greek side, where CO_2 showed the highest concentrations among the investigated samples, approach or even exceed the pCO_2 = 0 line.

The temperature *vs.* salinity (TDS) diagram (Fig. 6b) highlights the already mentioned relative high temperature and low salinity of the northern Bulgarian samples (<1000 mg/L), with respect to the more saline and lower temperature samples of the Greek sector. This geographical distribution is also in agreement with the temperature *vs.* SiO_2 diagram (Fig. 6d) since the hot samples from Bulgaria have high contents of SiO_2 and a T/SiO_2 ratio generally greater (>0.6) that those discharging in the Greek sector. This apparent contrasting result can be explained by the fact that SiO_2 from the Bulgarian samples is probably constrained by crystalline quartz, whereas in Greece more soluble silica phases in the Neogene sedimentary cover are involved in the water-rock interaction process. It is remarkable that most hot waters from Bulgaria

Table 3
Chemical and isotopic composition and N_2/Ar and N_2/Ne ratios of gas samples from the Strymon Valley. Gas contents are in % by vol. The carbon isotopic composition of CO_2 is expressed as $\delta^{13}C$ in ‰ *vs.* V-PDB. The Rc/Ra ratio is the measured $^3He/^4He$ ratio corrected on the basis of the He/Ne ratio in the studied gases divided by that of the air (1.39×10^{-6}).

No	Sample	Type	T	CO_2	N_2	CH_4	C_2H_6	Ar	O_2	He	Ne	H_2	H_2S	$\delta^{13}C\text{-}CO_2$	Rc/Ra	N_2/Ar	N_2/Ne
1	Biala voda strip	ex	27.0	30.72	64.21	0.000001	0.64	0.847	3.47	0.3398	0.0007800	<0.000001	<0.005			75.8	82,321
2	Kiustendil strip	ex	73.0	0.01	82.56	0.000020	21.97	1.305	15.85	0.0500	0.0010500	0.001500	<0.005			63.3	78,629
5	Slatino strip	ex	22.5	0.01	93.93	0.000003	0.82	1.462	4.59	0.5568	0.0010100	<0.000001	<0.005		0.3	64.2	93,000
7	Sapareva banja	free	96.5	0.01	92.05	0.000130	39.85	1.685	3.82	0.3015	0.0013900	0.200100	<0.005		0.26	54.6	66,223
9	Kozhuch	free	73.0	90.31	8.25	0.000047	17.51	0.009	1.13	0.0032	0.0000070	<0.000001	<0.005	−2.25		916.7	1,178,571
11	Spatovo strip	ex	33.4	0.01	94.59	0.000006	0.21	1.830	4.45	0.0494	0.0014600	0.001100	<0.005			51.7	64,788
13	Gradeschniza strip	ex	70.0	0.11	83.04	0.000001	0.53	1.210	16.75	0.0182	0.0009600	<0.000001	<0.005			68.6	86,500
16	Dolno Osenovo	free	58.0	0.01	95.89	0.000031	13.58	1.375	2.76	0.2286	0.0009500	<0.000001	<0.005			69.7	100,937
20	Dolmo Banja strip	ex	70.0	0.01	83.57	0.000006	2.89	1.431	15.38	0.0599	0.0009900	0.000500	<0.005			58.4	84,414
21	Kasicene	free	75.5	24.87	71.85	0.000025	13.12	1.275	1.38	0.1670	0.0009400	0.016900	<0.005	−9.37		56.4	76,436
23	Radmo Pole strip	ex	58.0	23.69	64.31	0.000007	4.32	0.985	10.83	0.0504	0.0008700	<0.000001	<0.005			65.3	73,920
24	Novi Iskar	free	24.0	31.42	67.13	0.000000	0.13	0.485	0.05	0.7687	0.0003600	<0.000001	<0.005	−3.44	0.07	138.4	186,472
25	Agistro 1 strip	ex	17.2	0.47	76.49	0.000050		1.781	21.26	0.0010	0.0012200	<0.000001	<0.005			43.0	62,697
26	Agistro 2	free	40.9	0.01	79.89	0.000400		1.500	18.60	0.0190	0.0007600	0.000670	<0.005		0.61	53.3	105,115
28	Sidirocastro T. strip	ex	43.8	66.28	25.79	0.000470		0.514	7.41	0.0000	0.0003500	<0.000001	<0.005			50.2	73,696
30	Sidirocastro 4	free	44.3	98.24	1.54	0.101737	0.69	0.035	0.08	0.0026	0.0000220	0.002148	0.005	−2.62	0.58	43.7	69,998
31	Sidirocastro strip	ex	41.9	72.09	21.65	0.006808	2.01	0.464	5.79	0.0000	0.0003400	<0.000001	<0.005			46.6	63,670
35	Sidirocastro piscine strip	ex	24.0	3.68	73.87	0.000466		1.602	20.84	0.0000	0.0011600	<0.000001	<0.005			46.1	63,684
36	Therma	free	48.0	98.27	1.63	0.000718	0.17	0.037	0.07	0.0002	0.0000260	0.000030	<0.005	−2.74	0.74	44.5	62,626
37	Therma 1	free	60.0	96.54	2.73	0.053971	5.02	0.013	0.04	0.0050	0.0000090	0.000143	<0.005	−0.70		207.5	303,542
38	Th 10(101)	free	58.5	99.24	0.69	0.004524	1.24	0.012	0.05	0.0012	0.0000080	0.000185	<0.005	−1.31	0.26	56.1	86,535
40	Therma O-2TS	free	50.0	99.36	0.61	0.004035	0.24	0.009	0.02	0.0012	0.0000050	0.000279	<0.005	−1.09	0.26	65.9	121,256
43	Levunovo	free	83.5	13.56	82.97	1.821820	30.70	1.463	0.19	0.0537	0.0008100	0.010170	<0.005	−3.90	0.54	56.7	102,432
45	Marikostinovo	free	39.1	6.69	28.26	60.414000		0.556	4.08	0.0129	0.0003800	0.004030	<0.005	−6.96	0.46	50.9	74,361
50	Lithotopos LI-1 strip	ex	39.0	10.57	69.86	0.002413	3.03	1.552	18.01	0.0280	0.0011600	0.000650	<0.005		0.57	45.0	60,228
51	Lithotopos strip	ex	16.8	6.03	56.55	36.402492		0.994	0.02	0.0003	0.0006800	0.000500	<0.005			56.9	83,164
58	Elephtere strip	ex	39.0	90.89	7.83	0.008664	2.24	0.158	1.12	0.0000	0.0001100	<0.000001	<0.005			49.6	71,148
59	Elephtere 1a	free	41.2	94.67	5.12	0.070344	9.23	0.029	0.02	0.0021	0.0000150	0.000343	<0.005		0.37	175.6	341,444
59b	Elephtere 1b	free	41.2	95.46	4.37	0.064654	7.95	0.027	0.02	0.0021	0.0000150	0.000095	<0.005	−1.49		163.7	291,518

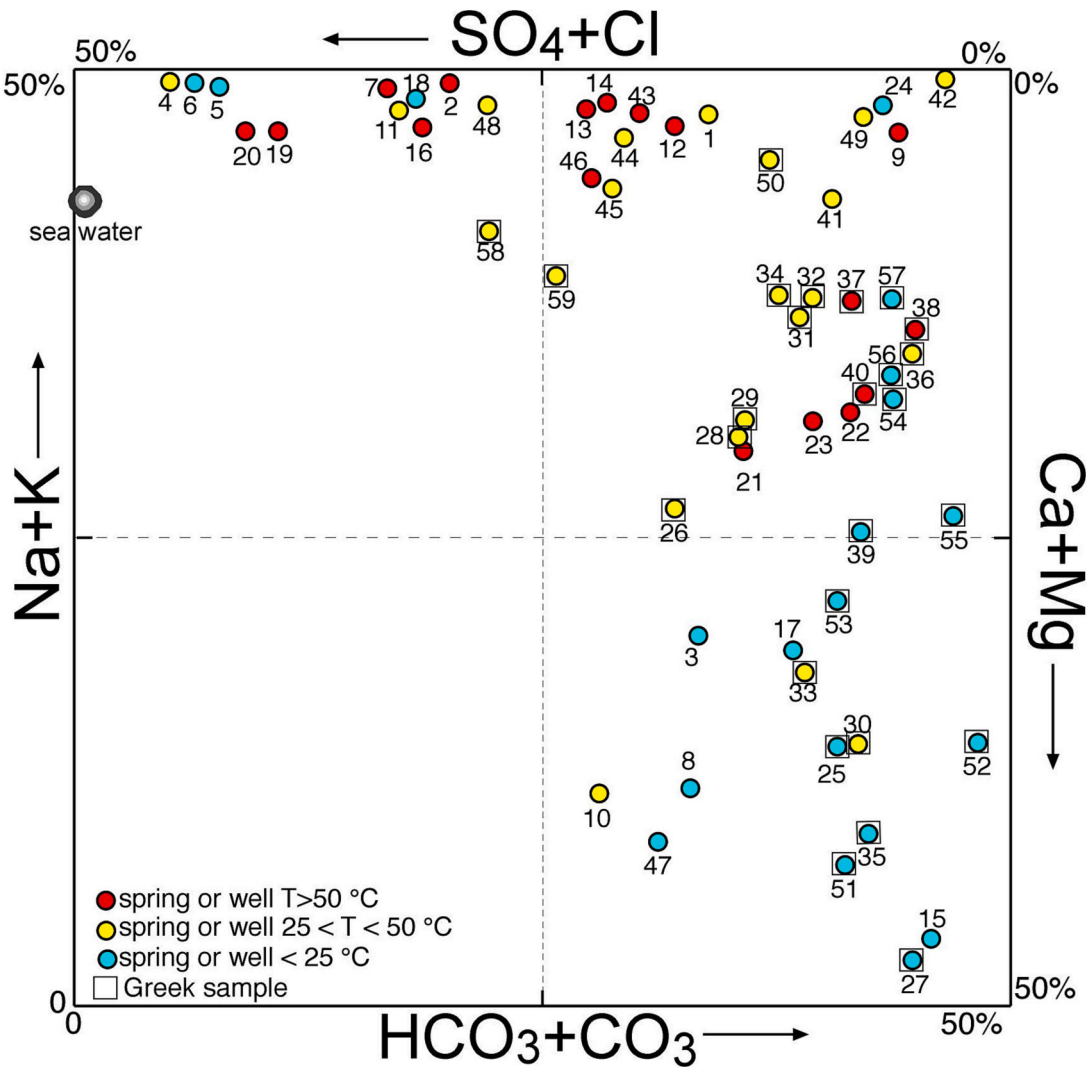

Fig. 2. Square diagram (Langelier and Ludwig, 1942) for the studied samples from the Strymon River Valley, subdivided on the basis of location and the outlet temperature.

have the (SO_4 + Cl) pair prevailing over that of (HCO_3 + CO_3) (Fig. 2). This is likely due to the fact that these waters circulate in the basement rocks where the presence of carbonate material is rather low, or calcite precipitation may occur at depth because of the high *p*H values, that favor the formation of CO_3^{2-} ions in solution and therefore, the secondary precipitation of veined-calcite.

In terms of minor and trace elements, some differences between the Bulgarian and Greek hot waters discharging in the SR valley can be highlighted. Setting aside the generally low NO_3 content, with the exception of two cold samples (#10 and #47), possibly affected by anthropic (agricultural) contamination, the concentration of NH_4 tends on average to be higher in the Bulgarian, suggesting a more reducing environment, than that of the Greek waters, although no Eh values are available. Fluoride contents up to 17 mg/L characterizes the Bulgarian waters whereas those from the Greek sector are always much lower. The different lithological features of the two areas play a key-role in the distribution of fluoride. The crystalline basement and granitic rocks host numerous F-bearing minerals (*e.g.* biotite, amphibole, muscovite; Gillberg, 1964; Koriting, 1974) and the presence of high *p*H favor the persistence of fluoride in the aqueous phase (*e.g.* Banks, 1997; Morland et al., 1997), particularly when Ca concentrations are rather low as it is the case of the Bulgarian waters that disfavor the precipitation of fluorite (CaF_2) (*e.g.* Chae et al., 2006 and references therein).

While the concentrations of lithophile (Li, B, Rb, Sr and Ba), chalcophile (Cd, Cu, Se and Zn) and siderophile (Ni and Cr) trace elements are rather similar in the studied waters, those of high field strength elements, such as W and Mo, evidence striking differences between the Bulgarian and Greek samples. Tungsten and Mo mainly occur as hexavalent cation with a ionic potential of 10.3 and tend to fully deprotonate the water molecule to form the oxy-anions (WO_4^{2-} and MoO_4^{2-}) in the aqueous phase, respectively (*e.g.* Grasselly, 1959). WO_4^{2-} and MoO_4^{2-} are relatively stable at alkaline pH, *e.g.*, Cao and Guo (2019) and Smedley and Kinniburgh (2017), respectively. Their geochemical behavior is supported by their relatively high concentrations, up to 165 (#7) and 23 (#13) μg/L (Table 2), respectively, in the high pH waters from Bulgaria whereas their contents in the Greek sector are significantly lower (Table 2). The source of W and Mo can be related to the crystalline basement and the granitic rocks (*e.g.* Blevin and Chappell, 1992) that dominate the northern part of SR while the southern part is mostly characterized by sedimentary deposits.

Arsenic is found in nature in two oxidation states (+3 and +5) and are soluble in a large range of pH and Eh (Bell, 1998). Although no speciation studies were carried out, it is to remark that high As contents were found in both the Bulgarian and Greek waters. They are indeed often characterized by concentrations higher than 10 μg/L, which is considered the maximum admittable concentrations for drinking waters. This limit is frequently overcome by the Bulgarian hot waters (up to 271 μg/L; #21) as well as by those from Greece, the latter being

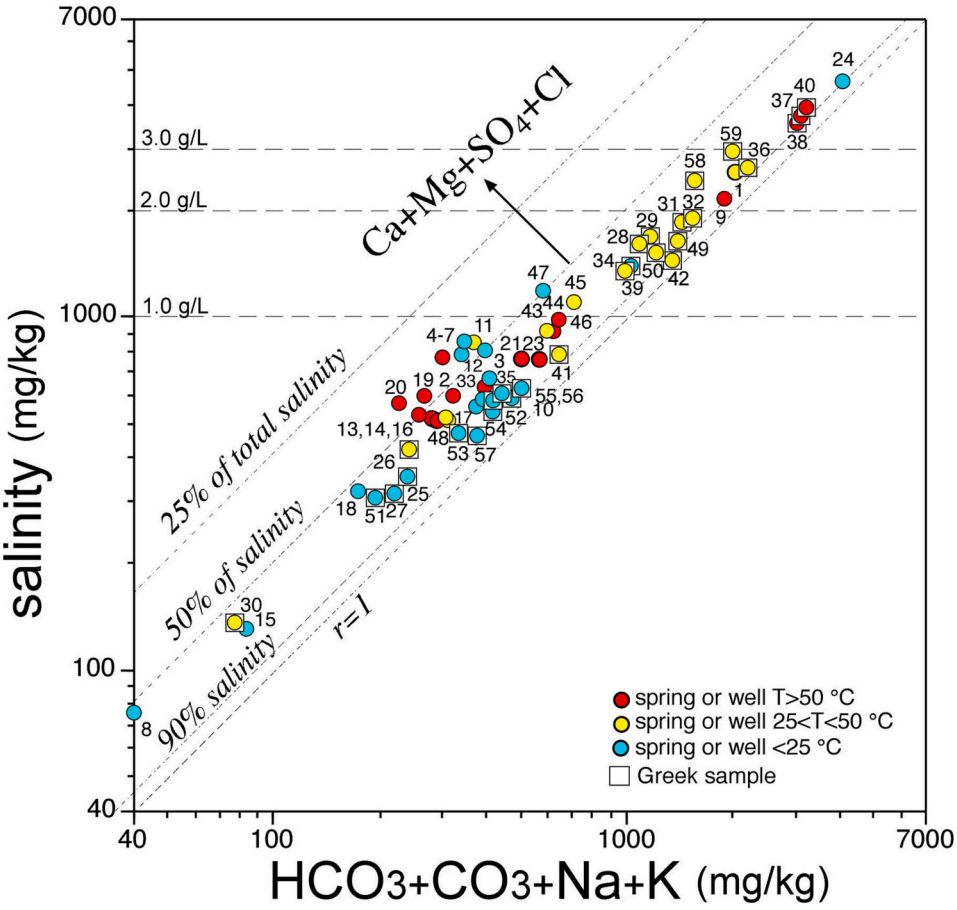

Fig. 3. Salinity *vs.* $HCO_3 + CO_3 + Na + K$ binary plot for the Strymon River valley waters.

characterized the higher contents shown by samples #36 and #59, with 911 and 741 μg/L, respectively. Most As-rich waters are associated with high TDS and/or *p*H values. The presence of arsenic is geogenic as also evidenced by Katsoyiannis and Katsoyiannis (2016) who analyzed several groundwaters not far from the study area. More investigations are requested to verify the source of arsenic, although this is beyond the aims of this work.

If the chemical composition of the gas phases is jointly discussed with that of the liquid phase, the Greek thermal springs of Nigrita (# 36–40), Sidirokastro (#25–35) and Elephtere (# 59), and some thermal samples straddling MML (# 9, #43), show the intimate correlation between high TDS and high Pco_2 values (not shown). This causes the occurrence of active travertine precipitation at the emergence orifices after CO_2 degassing, according to the following reactions:

$$2Ca^{2+} + 2HCO_3^- = CaCO_3 + H_2CO_3$$

$$H_2CO_3 = CO_2 + H_2O$$

All these characteristics suggest the presence, in the underground circulation paths of the Greek thermal springs, of Permian marble (Bonev et al., 2019) dissolution, as already reported in the literature (Mendrinos et al., 2010). The fact that CO_2 is related to the dissolution of carbonate material at depth is corroborated by the $^{13}C/^{12}C$ isotopic ratios (as $\delta^{13}C$ ‰), which vary from-3.9 ‰ (# 43) and −0.7 ‰ (# 37; Nigrita). These values are close to the expected value (around 0 ‰) for carbon deriving by the dissolution of carbonate deposit (*e.g.* Deines et al., 1974; Sano and Marty, 1995; Minissale, 2004; Clark, 2015).

As already discussed, most Bulgarian thermal and-cold-water discharges are Na-HCO_3 in composition at which a N_2-dominant gas phase of clear atmospheric origin (Fig. 4) is associated. The only hot spring near Sofia (# 21) where the carbon isotopic ratio in CO_2 is available, had a value of −9.37 ‰, clearly indicating the involvement of isotopically light organic CO_2 (*e.g.* Deines et al., 1974) and/or carbonate precipitation at depth able to fix in the lattice the dissolved heavy carbon-13 (*e.g.* Venturi et al., 2018).

A further relevant classification diagram to understand the origin of gases is the triangular plot where the relative concentrations of He(x10) are plotted with those of Ar and N_2/100 (Giggenbach et al., 1983). The diagram for the SR samples (Fig. 7) confirms what shown in Fig. 4, some gas samples (#9, 24, 37, 40, 59), prevalently located in southern Strymon, are indeed characterized by an extra-atmospheric source (metamorphic and/or organic) of N_2 (*e.g.* Javoy et al., 1984; Haendel et al., 1986; Jenden et al., 1988). The relative increase of radiogenic crustal He in the gas phase, of all thermal and hot samples, is related to the longer residence time of the parent water in the crust with respect to the cold samples that are located between the position of air and ASW along the N_2—Ar axis (Giggenbach et al., 1993).

6. Geothermometry

Geothermometry, *i.e.* the prediction of temperature at depth of a (geo)thermal reservoir by using chemical data in fluid phases, naturally discharging as thermal springs, is always a difficult task. The most significant chemical and physical processes that may occur and affect both fluid temperature and chemical composition along the deep rising path (s) before they emerge as thermal waters, are, as follows: *i*) fluid mixing from different aquifers at different temperatures, *ii*) dilution of hot deep

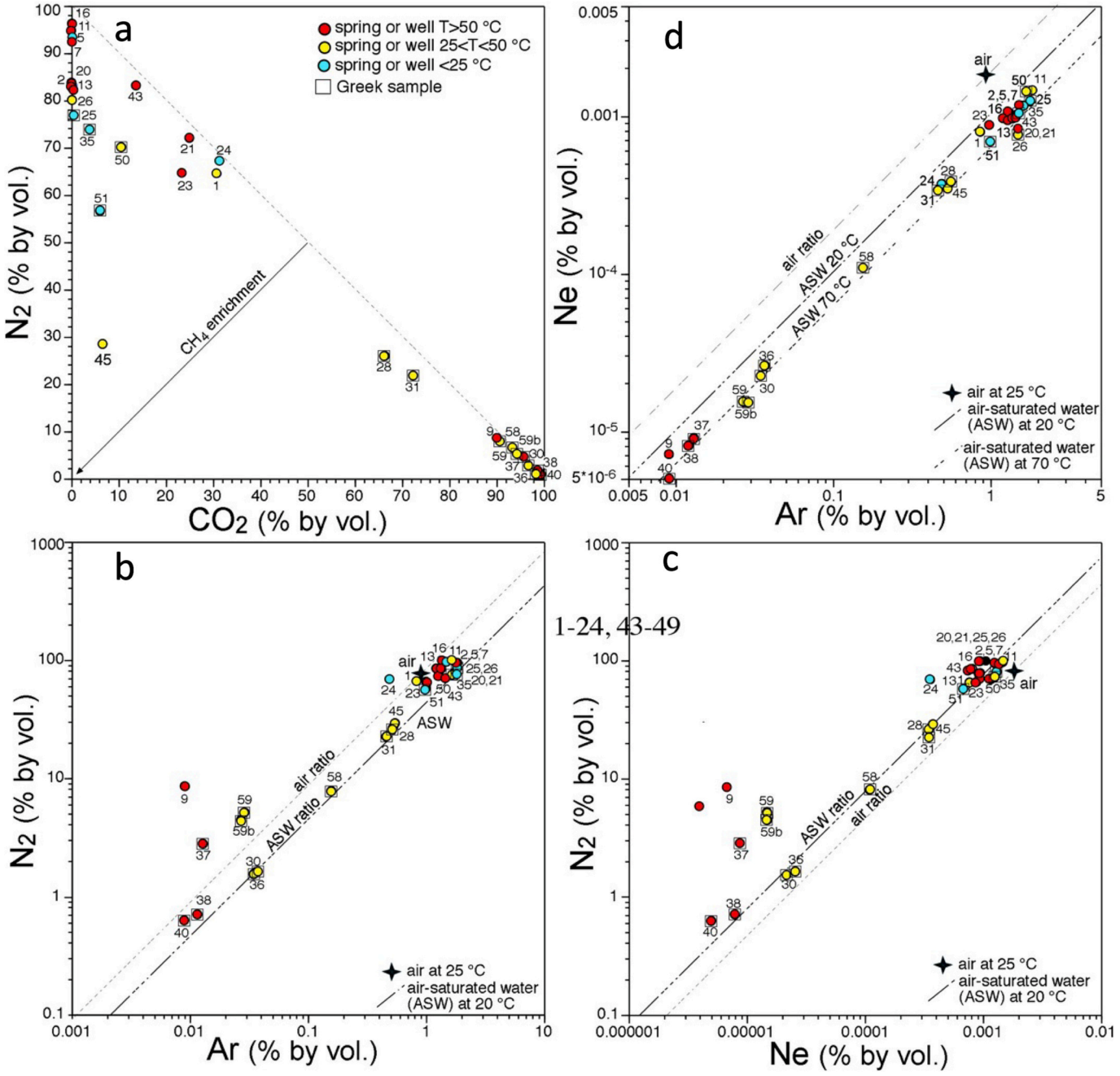

Fig. 4. Diagrams of N_2 *vs.* CO_2 (a), N_2 *vs.* Ar (b), N_2 *vs.* Ne (c) and Ne *vs.* Ar (d) binary diagrams for the Strymon River Valley gas samples.

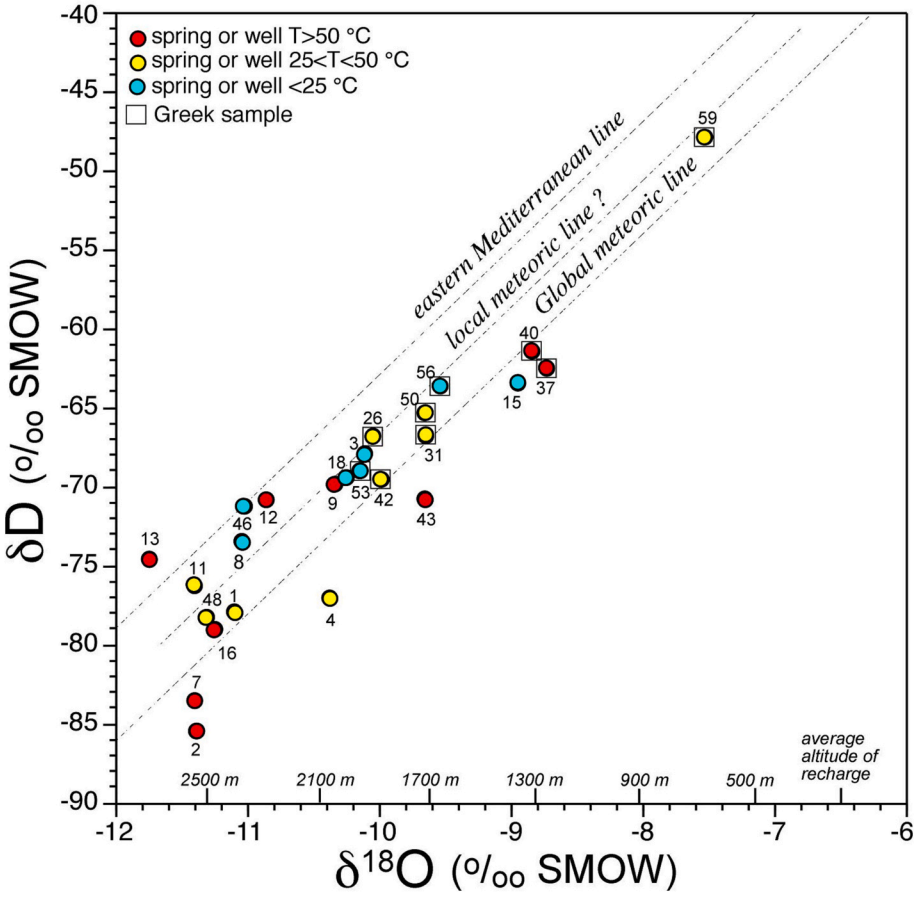

Fig. 5. δD *vs.* $\delta^{18}O$ binary diagram. The Global Meteoric Water Line (Craig, 1961) and the Eastern Mediterranean Water Line (Gat and Carmi, 1970) along with the supposedly local meteoric line are also drawn. The diagram shows on the x axis the likely average altitude of recharge of parent waters.

waters with cold descending meteoric waters and *iii*) re-equilibration of the dissolved components at lower temperature while approaching the surface. There is an extensive literature on this issue (*e.g.* Guo et al., 2017 and references therein) and the occasionally poor reliability of predicted deep temperature by using geothermometers. In this section, a qualitative approach to assess the geothermal potential of the Strymon basin, at least for power generation, was applied.

Previous geothermometric investigations for the Bulgarian waters are by Shterev and Penev (1991) and Shterev et al. (1995) while in the southern Greek sector temperature estimations were provided by *e.g.* Mendrinos et al. (2010); Li Vigni et al. (2021) and Dotsika et al. (2021). The several deep wells drilled for oil exploration, especially in the Greek sector (Karytsas, 1990), have demonstrated that the temperature at depth, even in the CO_2-rich area of Nigrita are due to a normal thermal gradient. In particular, at the 3651 m deep STR-1 well located about 10 km east of Nigrita, a temperature of 135 °C was recorded, approaching that estimated with isotopic geothermometer (150 °C) by Dotsika (1991). The bottom hole was still in the Miocene sediments. In the same area, borehole temperatures did not overcome 64 °C (Karydakis et al., 2005). In the Sidirokastro and Lithotopos-Iraklia thermal fields, up to 500 m wells and solute geothermometers (*e.g.* SiO_2, Na/K, Na/K/Ca, Na/Li, Mg/Li) provided temperature up to 65 to 100 °C, respectively. Such relatively low temperatures were also measured and/or estimated at the Agistro and Ivira thermal fields (Karydakis et al., 2005; Dotsika et al., 2021). Higher geothermal gradients were evidenced at Separeva, Levunovo and Sandanski but at 500 m depth the borehole temperatures were at about 110 °C, suggesting typical convective hydrothermal systems.

To the best of our knowledge, gas geothermometry has not been applied to the Bulgarian and Greek gases discharging in the SR valley. Thus, temperature estimates inferred from the gas chemical dataset (Table 3) are discussed here below and compared with this direct temperature measurement.

In Fig. 8, a binary plot of the $\log(\chi CH_4/\chi CO_2)$ *vs.* the $\log(\chi H_2/\chi Ar)$ (Giggenbach, 1993) is reported, where χ is the mole fraction of plotted components. The diagram is constrained, at temperatures of geothermal interest, by the rock buffer given by the couple Fe^{2+}/Fe^{3+}. The H_2/H_2O ratio ($RH = \log(fH_2/fH_2O)$ where f stands for fugacity at boiling conditions) is assumed to be independent by temperature, and fixed at a value of −2.8 (Giggenbach, 1987). The relative equilibrium curve at boiling conditions limits a *two phase* grey area where the liquid and vapor phases are coexisting. The large white area, delimited to the left of the boiling curve, and the line, where the gas compositions are constrained by the *calcite-anhydrite* buffer, allow to make the following considerations: *i*) the gas samples in the source area, if deriving from geothermal systems, are very far from the boiling line, in strong oxidizing conditions where H_2 is eventually converted to H_2O and/or, more likely, *ii*) the addition of "shallow" biogenic CH_4, not deriving from high temperature reaction such as $CO_2 + 4H_2 = CH_4 + 2H_2O$ (Fischer-Tropsch-type), as commonly occurring in many gas discharging areas (*e.g.* Venturi et al., 2019). Both these conditions, especially if jointly operating, cause the shifting of samples in an area of clear disequilibrium. Actually, the iso-temperature lines shown in the diagram which branch off from the boiling curve, represent the expected relative proportions of H_2, CO_2, CH_4 and Ar at different RH values. Apart from the thermal sample #45, probably affected by incorrect H_2 or Ar values, all

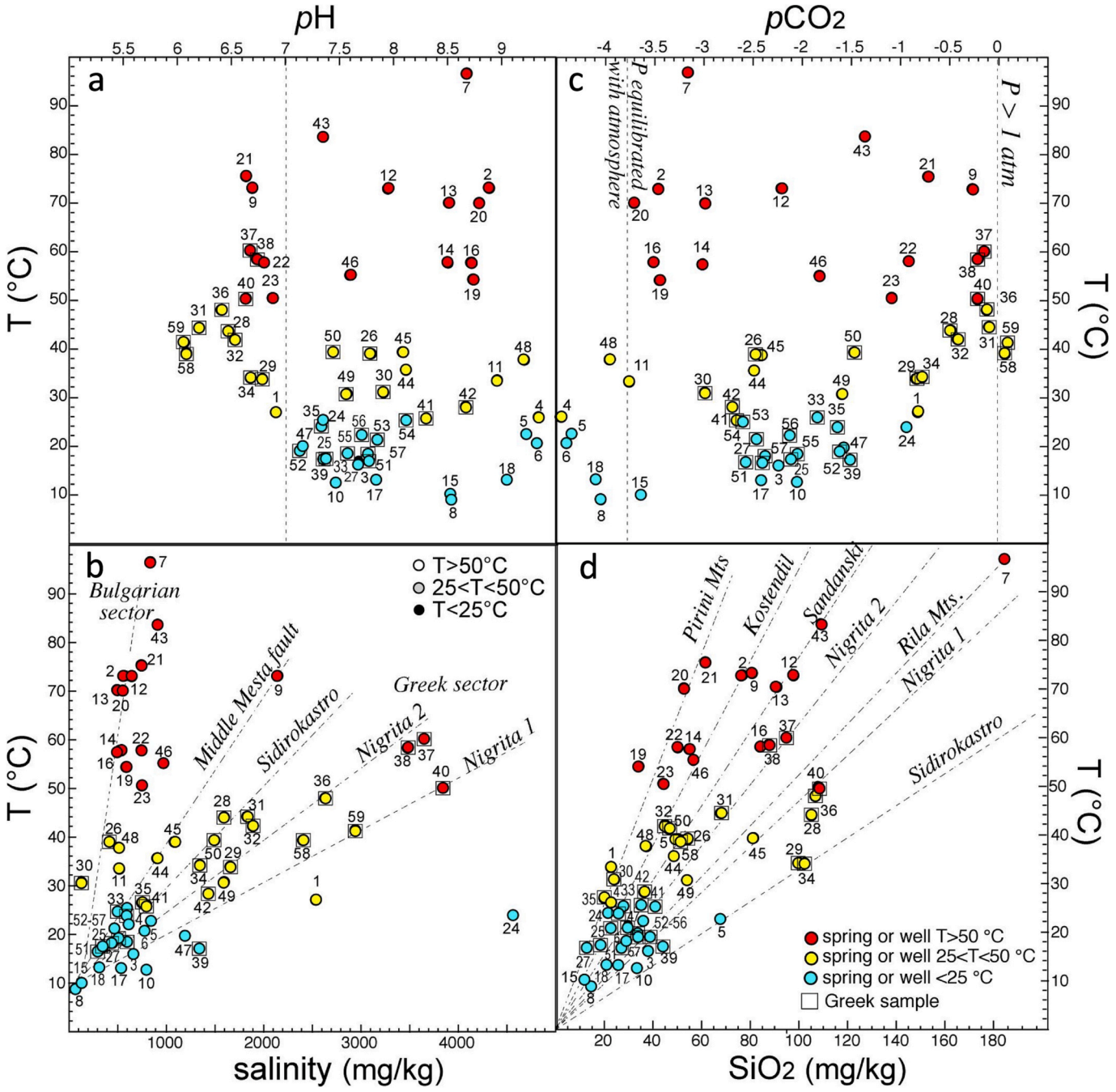

Fig. 6. Multiple diagram of temperature *vs.* pH (a), salinity (as TDS) (b), pCO_2 (c), and SiO_2 (d).

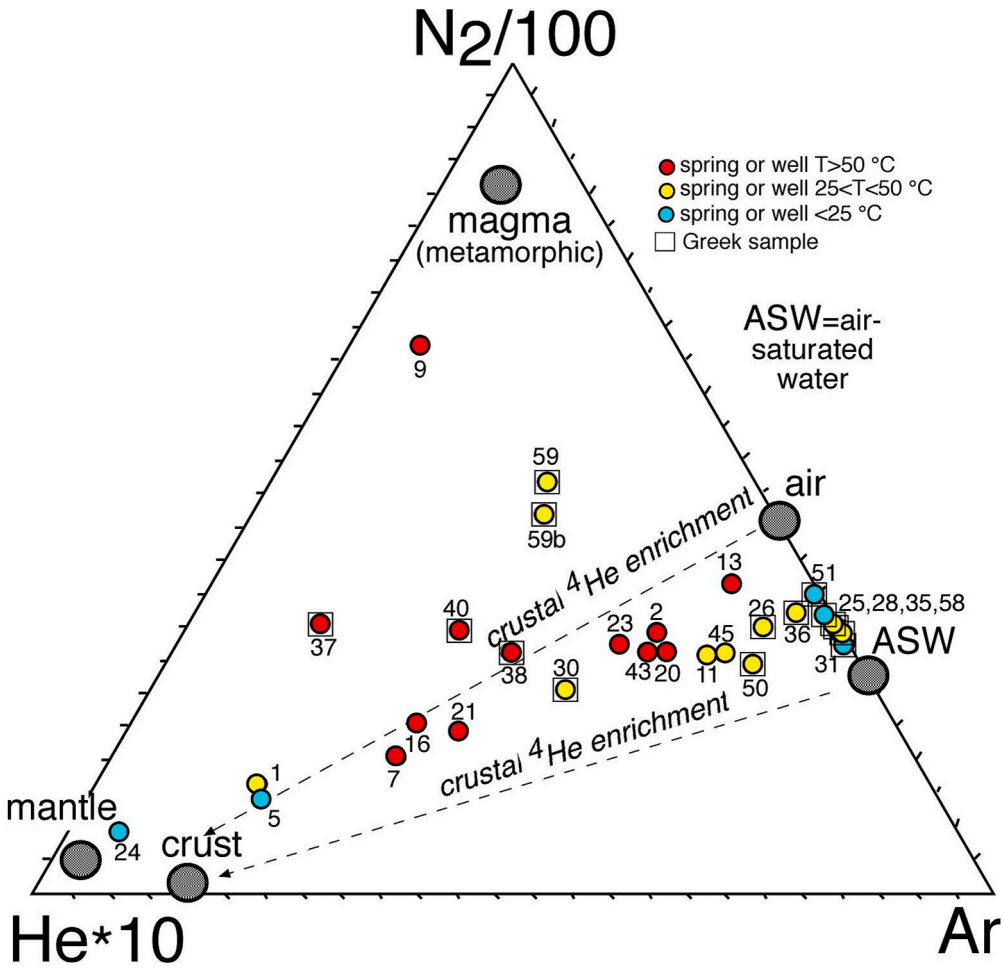

Fig. 7. Ternary diagram of N_2(/100)-He(10×)-Ar (Giggenbach et al., 1983) for the investigated gas samples.

the remaining samples show temperatures <150 °C, and most of them are <100 °C. It is interesting to note that several samples are aligned at about 70 °C, a temperature suggested by several samples in the Ne—Ar diagram in Fig. 4 (#11, #30, #37, #50, #59). Consequently, both solute and gas geothermometers indicate that along the SR valley the presence of high temperature is unlikely. However, thermo-economic evaluations can be taken into account to install Organic Rankine Cycle (ORC) plants as they operated with different working fluids at temperature even lower than 100 °C (*e.g.* Quolin et al., 2013).

7. Relation between thermal springs and tectonics

Setting aside those areas characterized by the presence of active or recent volcanism where the presence of thermal emergences at surface is triggered by the presence of shallow magmas in the crust, such as *e.g.* Yellowstone Park with its >20,000 thermal emissions (Lowenstern et al., 2015), in general the presence of thermal spring is not a common occurrence on Earth. Where present, especially in stable cratonic areas, they are always associated with regional faults, such as the San Andreas fault in the U.S. (Jenden et al., 1988) or the Anatolian fault in Turkey (De Leeuw et al., 2010). Fault-related and/or "intracratonic"-related thermal spring waters have the following features (Minissale et al., 2000): *i*) variable (low-to-medium) salinity; particularly low when circulating throughout crystalline formations; *ii*) marked Na-HCO_3 composition where carbon is mostly derived from atmospheric or bacterial (soil-derived) CO_2; *iii*) meteoric origin of the parent water with relatively small ^{18}O shifts with respect to the global meteoric line, *iv*) nitrogen (and or methane) as the main associated gas phase; *v*) high crustal radiogenic ^4He due to long circulation paths before discharging at the surface and *vi*) very low $^3He/^4He$ ratio because of the presence of high crustal ^4He.

Considering the chemical and isotopic composition and the estimated equilibrium temperatures of the thermal springs and gas discharges in SR valley, active high temperature hydrothermal systems, as previously mentioned, are not expected. Therefore, it is reasonable to suppose that the presence of such large quantity of thermal emergences, roughly N-S oriented, is intimately related to the complex tectonic structure of the Strymon basin and surrounding areas. As we showed above (see Fig. 1), the Strymon valley is surrounded by two high crystalline massifs and other small ranges where precipitation is >1 m/y and abundant snow in winter. These running waters are forced to topographically move to the valley and therefore, the presence of rising thermal waters from depth should strongly be hampered by both descending rainfall, melted snow and surface waters, though this is apparently not the case. A possible interpretation of the fluid circulation across SR is schematically shown in Fig. 9.

SR is not a typical sedimentary basin being quite asymmetric, with the bounding Strymon low angle detachment fault from the East (Georgiev et al., 2010) crosscut by steep (60–80°) normal fault systems (Fig. 4) that gradually decrease southwards and increasing extension in the Serres graben (Shterev et al., 1995). The division is marked by MML, north of which marine sediments are completely absent. The E-W-oriented MML seems to act as a boundary in terms of both water and gas chemistry. The presence of shallow marine sediments and deep-buried

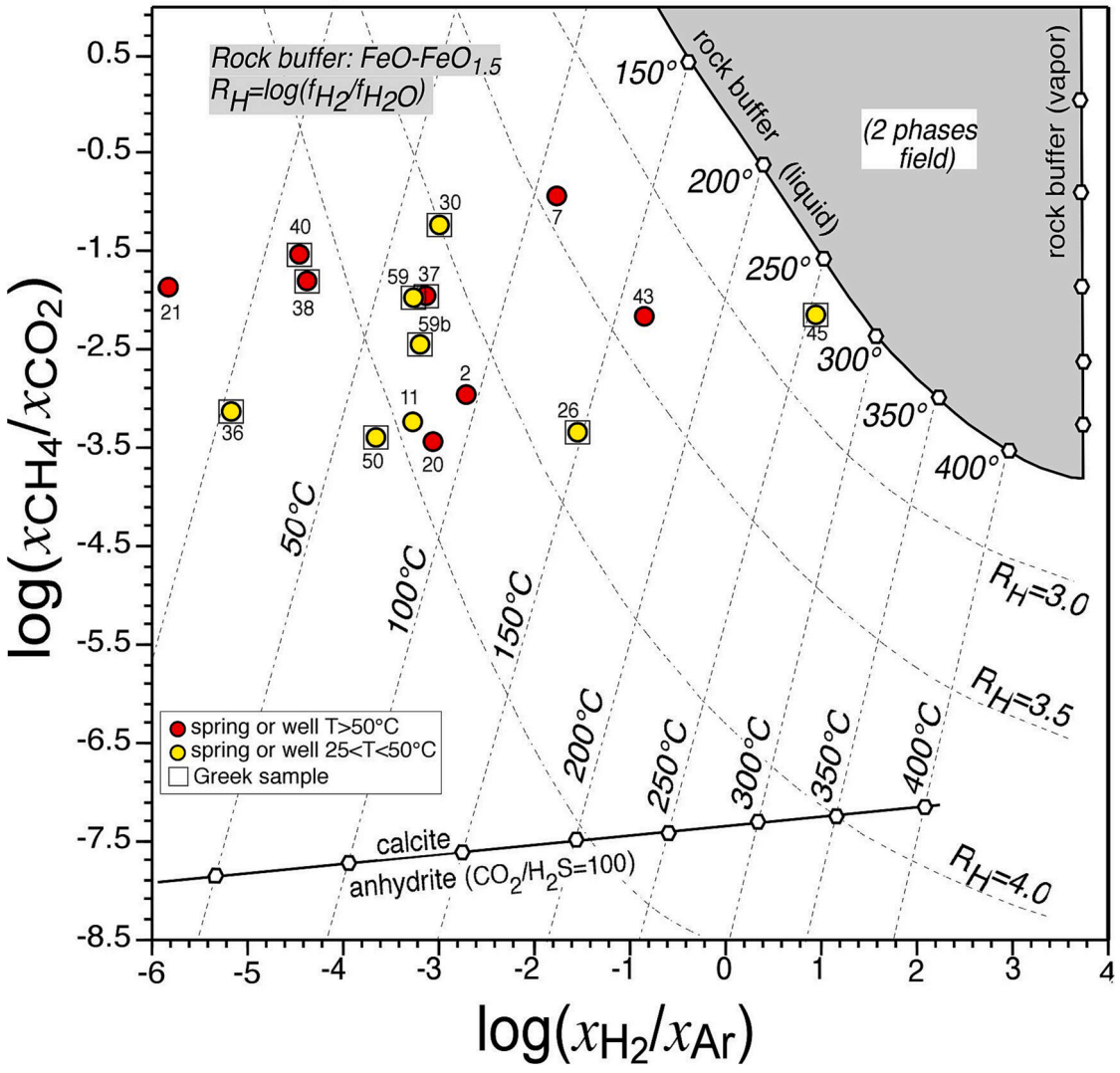

Fig. 8. Binary diagram of $\log(\chi CH_4/\chi CO_2)$ *vs.* the $\log(\chi H_2/\chi Ar)$ from Giggenbach (1993) where χ is the mole fraction of relative components. See text for details.

marble (Fig. 1) tends to increase the TDS values as well as CO_2 in the discharging respectively, particularly in the Greek sector.

Despite the different gas and water composition between the Bulgarian and Greek samples, the role played by the Strymon structure to host ascending branches of deep convective circulations that originate in the surrounding mountain ranges has to be critical. Consequently, the reason of this is likely related to tectonic implications. In spite of the main NNW-SSE direction of most faults (Fig. 1) bordering the structure, there are also many E-W-oriented faults including MML. It seems thus reasonable to suppose that in places, where the hot deep aquifers are shallower and affected by one of the several fault systems occurring in the area, especially at low elevations, the hot fluids are able to emerge as thermal springs. It can also be hypothesized that the deep fluids rise up fast enough to prevent the possibility of silica precipitation at cooler temperature. Where deep wells were drilled, *e.g.* Sandanski, around spring areas, the measured temperatures are indeed not much higher than those of the springs or those computed with the SiO_2 geothermometers (Mendrinos et al., 2010). The only significant difference in terms of SiO_2 is related to the sample #7 (Table 1), which showed a concentration as high as 185 mg/L. However, it is to mention that the associated gas chemistry is N_2-rich and also characterized by an alkaline *p*H which increases the SiO_2 solubility. This is also supported by the thermal wells drilled at Separeva where at around 500 m the log temperatures were clustering around 110 °C (Shterev et al., 1995). In our opinion, this further allows to hypothesize that high-T geothermal systems along the SR valley should not be occurring.

Regarding the thickness of the crust involved in the local active tectonics, the $^3He/^4He$ (as Rc/Ra) ratio, a very strong parameter to identify rising mantle gases (*e.g.* Sano and Fischer, 2013 and references therein), was determined in selected samples (Table 3). The values ranged from 0.07 R/Ra (#24) to 0.74 (#36) and they are similar to those measured by Piperov et al. (1994) and Magro et al. (2010). Considering that the helium ratios were corrected for air contamination, and that the presence of mantle degassing is certain for Rc/Ra values >0.2 (O'Nions and Oxburgh, 1988; Marty and Jambon, 1987), it seems possible that the Strymon river is constrained to flow southward by a relevant transpressive structure, able to drain mantle helium (<10 % or less) to the surface, as also suggested by Magro et al. (2010). It has to be reminded that the youngest volcanic event in Bulgaria occurred at about 12 Ma along the Strymon Valley (Georgiev et al., 2013; Eleftheriadis and Staikopoulos, 1997; Nisi et al., 2013). Unfortunately, no helium isotopes are available for this sample.

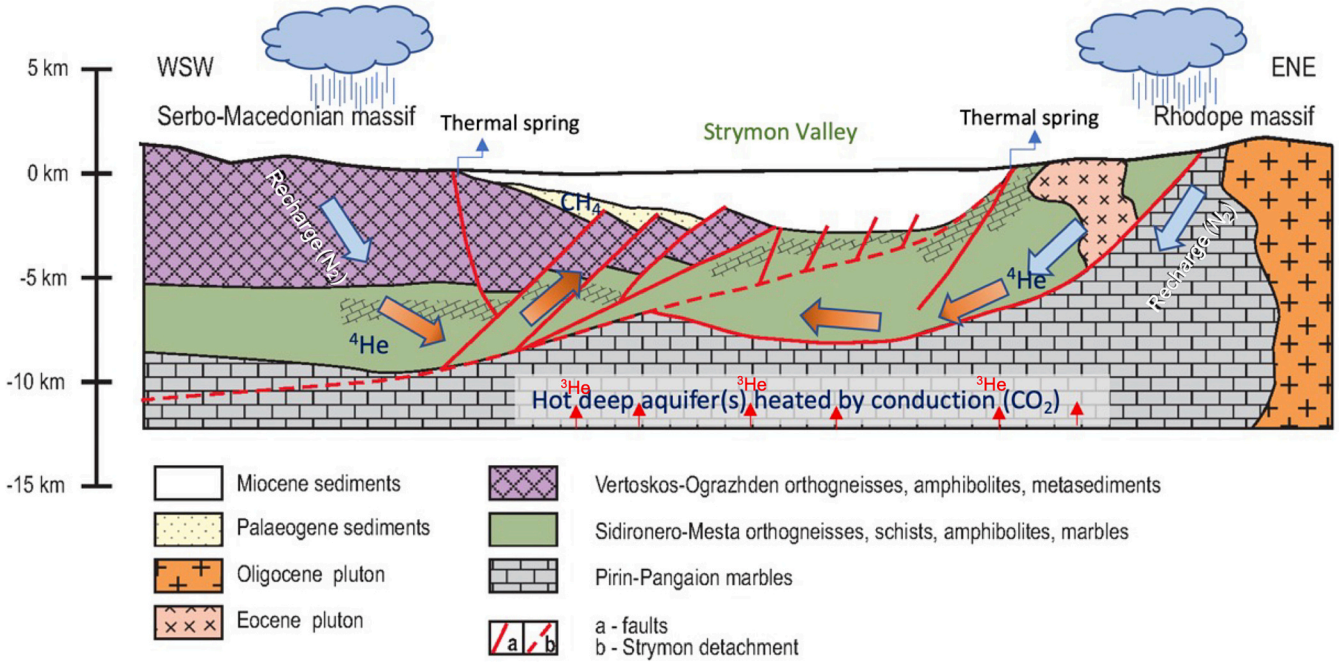

Fig. 9. Geochemical conceptual model of fluid circulation along the Strymon Valley. See text for details. (For interpretation of the references to colour in this figure, the reader is referred to the web version of this article.)

8. Conclusions

The geochemical and isotopic features of the fluid discharges along the SR valley have highlighted important differences between the Bulgarian and Greek sector. In the Greek sector several deep wells, originally drilled for oil exploration, registered temperatures related to normal thermal gradients and typical of stable cratonic areas. This implies that the presently discharging thermal springs are not related to the presence of magmatic intrusions or shallow hydrothermal systems. In the Bulgarian sector, the shallow wells drilled near the emergences of the thermal springs, show an apparently higher local thermal gradient (Shterev et al., 1995). The gas phase chemistry associated with the highest temperature springs of Bulgaria (*i.e.* Separeva Banja # 7), with the exception of that discharging at Kohzuh volcano, is, in most cases, characterized by N_2 (often >90 %), a clear meteoric origin, a high He concentration and a small ^{18}O-shift of the liquid phase, suggesting that thermality is likely not related to significantly anomalous geothermal gradients. Accordingly, the tectonic setting seems to be the only driving force to explain the relatively high number of thermal springs. This is well supported by the very high number of fault systems affecting the Rhodope and Serbo-Macedonian crystalline blocks. A geochemical conceptual modelling model able to explain the fluid circulation patterns across the SR valley is schematically shown in Fig. 9. The Strymon structure governs and drives the meteoric waters (blue arrows in Fig. 9), infiltrating through the crystalline massifs, to ascend in convective branches along the many NW-SE-oriented faults, possibly at the intersection with E-W faults, parallel to MML. The infiltrated rainfall heats up under roughly normal thermal gradients (orange arrows in Fig. 9) although, being the deep fluid circulation paths locally occurring through Hercynic and Alpine granitic intrusions typically rich in heat producing radiogenic elements (Th, U, K), a contribution by radioactive energy in heating the deep circuits cannot be excluded (Artemieva et al., 2017). The formation of the SR valley can be attributed to the geodynamics of the Aegean domain (Philippon et al., 2014) as well as to the arrangement of the involved plates (Anatolian, Apulian, African and Eurasian) due to subduction(s) and rotation processes and gravity spreading of the continental lithosphere that had been thickened during the Alpine collision (Gautier et al., 1999).

Declaration of competing interest

The authors declare that they have no known competing financial interests or personal relationships that could have appeared to influence the work reported in this paper.

Data availability

No data was used for the research described in the article.

Acknowledgements

We do wish to dedicate this work to P. Petrov who helped us in both his explanations about the geothermal systems of Bulgaria and his help in the field. N. Piperov is kindly thanked for his assistance during the field work. R. Raicheva gently prepared the figure of the conceptual model. The Editor and the three reviewers are kindly thanked for their help and constructive comments and suggestions that improved an early version of the manuscript.

References

Ambraseys, N.N., 2001. The Kresna earthquake of 1904 in Bulgaria. Ann. Geofis. 44, 95–117.

Andritsos, N., Arvanitis, A., Papachristou, M., Fytikas, M., Dalambakis, P., 2010. Geothermal activities in Greece during 2005–2009. In: Proc. 2010 World Geothermal Congress, 25–29 Apr., Bali, Indonesia, pp. 1–10.

Andritsos, N., Dalabakis, P., Karydakis, G., Kolios, N., Fytikas, M., 2011. Characteristics of low-enthalpy geothermal applications in Greece. Renew. Energy 36, 1298–1305.

Antić, M., Peytcheva, I., von Quadt, A., Kounov, A., Trivic, B., Serafimovski, T., Tasev, G., Gerdjikov, I., Wetzel, A., 2015. Pre-Alpine evolution of a segment of the North-Gondwanan margin: Geochronological and geochemical evidence from the central Serbo-Macedonian Massif. Gondwana Res. 36, 523–544. https://doi.org/10.1016/j.gr.2015.07.020.

Artemieva, I.M., Thybo, H., Jakobsen, K., Sorensen, N.K., Nielsen, L.S.K., 2017. Heat production in granitic rocks: Global analysis based on a new data compilation GRANITE2017. Earth Sci. Rev. 172, 1–26.

Arvanitis, A., Dotsika, E., Kolios, N., 2016. Geochemical characteristics of the geothermal fluids in the Akropotamos area (Macedonia, northern Greece). Bull. Geol. Soc. Greece 50, 596–605.

Atanasova, S., Bojidar, Mavrudchiev V., van Quadt, A., Peytcheva, I., Georgiev, S., 2004. Petrology and geochemistry of lamprophyric dykes in the Vitosha pluton. In: Bulgar. Geol. Soc. Ann Sci. Conf. "Geology 2004", vol. 16, pp. 100–102.

Atanasova-Vladimirova, S., von Quadt, A., Marchev, P., Peytcheva, I., Piroeva, I., Mavrudchiev, B., 2010. Petrology and geochronology of the Vitosha volcano-plutonic edifice, Western Srednogorie, Bulgaria. In: 19th Congress Carpathian-Balkan Geol. Assoc., 23–26 Sept., Thessaloniki (Greece).

Banks, D., 1997. Hydrogeochemistry of Milstone Grit and Coal Measures groundwaters, south Yorkshire and north Derbyshire, UK. Quarterly J. Engineer. Geol. 30 (2S7-280).

Bell, F.G., 1998. Environmental Geology: Principles and Practice. Blackwell Science, London, pp. 487–500.

Bencini, A., 1985. Applicabilità del metodo dell'Azometina-H alla determinazione del boro nelle acque naturali. Rend. Soc. It. Mineral. Petrol. 40, 311–316 (In Italian with English abstract).

Benderev, A., Hristov, V., Bojadgieva, K., Mihailova, B., 2016. Thermal waters in Bulgaria. In: Papic, P. (Ed.), Mineral and Thermal Waters of Southern Europe. Springer, pp. 47–64.

Blevin, P.L., Chappell, B.W., 1992. The role of magma sources, oxidation states and fractionation in determining the granite metallogeny of eastern Australia. In: Earth and Environmental Science Transactions of The Royal Society of Edinburgh 83, 2nd Hutton Symposium: The Origin of Granites and Related Rocks, pp. 305–316.

Bojadgieva, K., Hristov, H., Berova-Andonova, A., Benderev, A., Hristov, V., 2015. Geothermal update for Bulgaria (2010–2014). In: Proc. 2015 World Geothermal Congress, 19–25 Apr., Melbourne, Australia, pp. 19–25.

Bonev, N., Burg, J.-P., Ivanov, Z., 2006. Mesozoic–Tertiary structural evolution of anextensional gneiss dome—the Kesebir–Kardamos dome, Eastern Rhodope (Bulgaria–Greece). Int. J. Earth Sci. 95, 318–340. https://doi.org/10.1007/s00531-005-0025-y.

Bonev, N., Moritz, R., Borisova, M., Filipov, P., 2019. Therma–Volvi–Gomati complex of the Serbo-Macedonian Massif, northern Greece: a Middle Triassic continental margin ophiolite of Neotethyan origin. J. Geol. Soc. 176, 931–944. https://doi.org/10.1144/jgs2017-130.

Brun, J.P., Sokoutis, D., 2007. Kinematics of the southern Rhodope core complex (North Greece). Intl. J. Earth Sci. 96, 1079–1099.

Burchfiel, B.C., Nakov, R., Tzankov, T., 2003. Evidence from the Mesta half-graben, SW Bulgaria, for the Late Eocene beginning of Aegean extension in the Central Balkan Peninsula. Tectonophysics 375, 61–76.

Burg, J., 2012. Rhodope: From Mesozoic convergence to Cenozoic extension. Review of petro-structural data in the geochronological frame. In: Skourtsos, E., Lister, S.G. (Eds.), The Geology of Greece, Journal of the Virtual Explorer. ISSN: 1441-8142, Electronic Edition, vol. 42. paper 1.

Burg, J.-P., Ricou, L.-E., Ivano, Z., Godfriaux, I., Dimov, D., Klain, K., 1996. Syn-metamorphic nappe complex in the Rhodope Massif. Structure and kinematics. Terra Nova 8, 6–15. https://doi.org/10.1111/j.1365-3121.1996.tb00720.x.

Cao, Y., Guo, Q., 2019. Tungsten speciation and its geochemical behavior in geothermal waters: a review. E3S Web Conferences 98 (07005), 3–5.

Capasso, G., Inguaggiato, S., 1998. A simple method for the determination of dissolved gases in natural waters. Appl. Geochem. 13, 631–642.

Chae, G.-T., Jun, S.-T., K, M.-J., Kim, Y.-S., Mayer, B., 2006. Batch dissolution of granite and biotite in water: implication for fluorine geochemistry in groundwater. Geochem. J. 40, 95–102.

Clark, I., 2015. Groundwater Geochemistry and Isotopes. CRC Press, Boca Raton (FL), p. 456.

Clark, I.D., Fritz, P., 1997. Environmental Isotopes in Hydrogeology, 2nd ed. CRC Press, Boca Raton, FL, USA (pp. 55, 117, 210–212).

Coleman, M.L., Sheperd, T.J., Durham, J.J., Rouse, J.E., Moore, G.R., 1982. Reduction of water with Zinc for Hydrogen isotope analysis. Analyt. Chem. 54, 993–995.

Craig, H., 1961. Isotopic variations in meteoric waters. Science 133, 1702–1703.

Craig, H., Lupton, J.E., Horibe, Y., 1978. A mantle helium component in Circum-Pacific volcanic gases: Hakone, the Marianas, and Mt. Lassen. In: Alexander, E.G., Ozima, M. (Eds.), Terrestrial Rare Gases, Adv. Earth Planet. Sci, vol. 3, pp. 3–16.

D'Alessandro, W., Kyriakopoulos, K., 2013. Preliminary gas hazard evaluation in Greece. Nat. Hazards. https://doi.org/10.1007/s11069-013-0789-5.

De Leeuw, G.A.M., Hilton, D.R., Gulec, N., Mutlu, H., 2010. Regional and temporal variations in $CO_2/^3He$, $^3He/^4He$ and $\delta^{13}C$ along the North Anatolian Fault Zone, Turkey. Appl. Geochem. 25, 524–539.

Deines, P., Langmuir, D., Harmon, R.S., 1974. Stable carbon isotope ratios and the existence of a gas phase in the evolution of carbonate groundwaters. Geochim. Cosmochim. Acta 38, 1147–1164.

Dinter, D., Royden, L., 1993. Late Cenozoic extension in northeastern Greece-Strymon Valley detachment system and Rhodope metamorphic complex. Geology 21, 45–48.

Dotsika, E., 1991. Utilisation du geothermometre isotopique sulfate-eau en milieux de haute temperature sous influence marine potentielle: les systems geothermaux de Grece, These en Science. Univ. Paris-Sud (184 pp.).

Dotsika, E., Dalampakis, P., Spyridono, E., Diamantopoulos, G., Karalis, P., Tassi, M., Raco, B., Arvantis, A., Kolios, N., Michelot, J.L., 2021. Chemical and isotopic characterization of the thermal fluids emerging along the North-Northeastern Greece. Sci. Rep. 11, 16291. https://doi.org/10.1038/s41598-021-95656-6.

Eleftheriadis, G., Staikopoulos, G., 1997. Upper Miocene volcanicrocks at Neo Petrisi, Central Macedonia (N. Greece). Geologica Balcanica 27, 49–54.

Epstein, S., Mayeda, T., 1953. Variation of oxygen-18 content of waters from natural sources. Geochim. Cosmochim. Acta 4, 213–224.

Evans, W.C., White, L.D., Rap, P., 1998. Geochemistry of some gases in hydrothermal fluids from the southern Juan de Fuca ridge. J. Geophys. Res. 15, 305–313.

Facca, G., Tonani, F., 1967. The self-sealing geothermal field. Bull. Volcanol. 30, 271–273.

Florinsky, I.V., 2016. Digital Terrain Analysis in Soil Science and Geology. Elsevier Science Publish, Academic Press, San Diego (U.S.) (506 pp.).

Gat, J.R., Carmi, I., 1970. Evolution of the isotopic composition of atmospheric waters in the Mediterranean Sea area. J. Geophys. Res. 75, 3032–3048.

Gautier, P., Brun, J.P., Moriceau, R., Sokoutis, D., Martinod, J., Jolivet, L., 1999. Timing, kinematics and cause of Aegean extension: a scenario based on a comparison with simple analogue experiments. Tectonophysics 315, 31–72.

Georgiev, N., Pleuger, J., Froitzheim, N., Sarov, S., Jahn-Awe, S., Nagel, T.J., 2010. Separate Eocene–Early Oligocene and Miocene stages of extension and core complex formation in the Western Rhodopes, Mesta Basin, and Pirin Mountains (Bulgaria). Tectonophysics 487, 59–84. https://doi.org/10.1016/j.tecto.2010.03.009.

Georgiev, S., Marchev, P., Peitcheva, I., von Quadt, A., Vaselli, O., 2013. Miocene extensional magmatic activity along Strymon valley and Doyran region, SE Europe. Acta Vulcanol. 25, 153–168.

Giggenbach, W.F., 1975. A simple method for the collection and analysis of volcanic gas samples. Bull. Volcanol. 39, 132–145.

Giggenbach, W.F., 1987. Redox processes governing the chemistry of fumarolic gas discharges from White Island, New Zealand. Appl. Geochem. 2, 143–161.

Giggenbach, W.F., 1991. Chemical techniques in geothermal exploration. In: D'Amore, F. (Ed.), Application of Geochemistry in Geothermal Reservoir Develop. UNITAR, New York, pp. 253–273.

Giggenbach, W.F., 1993. Redox control of gas compositions in Philippine volcanic-hydrothermal systems. Geothermics 22, 575–587.

Giggenbach, W.F., Gonfiantini, R., Jangi, B.L., Truesdell, A.H., 1983. Isotopic and chemical composition of Parbaty Valley geothermal discharges, NW-Himalaya. Geothermics 12, 199–222.

Giggenbach, W.F., Sano, Y., Wakita, H., 1993. Isotopic composition of helium, and CO_2 and CH_4 contents in gases produced along the New Zealand part of a convergent plate boundary. Geochim. Cosmochim. Acta 57, 3427–3455.

Gillberg, M., 1964. Halogens and hydroxyl contents of micas and amphiboles in Swedish granitic rocks. Geochim. Cosmochim. Acta 28, 495–516.

Glavcheva, R., Matova, M., 2010. 120th anniversary of seismology in Bulgaria: milestones, development and achievements. Boletin de Geologia of Colombia 36, 125–158.

Grasselly, G., 1959. The role and significance of the complex anionic potentials in the geochemistry: part III: the characterization of the relative stabilities of the complex silicate anions by the ψ/SiO_4 potentials. Acta Mineral. Petrogr. 12, 41–49.

Guo, Q., Pang, Z., Wang, Y., Tian, Jiao, 2017. Fluid geochemistry and geothermometry applications of the Kangdinghigh-temperature geothermal system in eastern Himalayas. Appl. Geochem. 81, 63–85.

Haendel, D., Mohle, K., Nitzsche, H.M., Stihl, G., Wand, U., 1986. Isotopic variations of the fixed nitrogen in metamorphic rocks. Geochim. Cosmochim. Acta 50, 749–758.

Hristov, V., 1993. Application of chemical geothermometers to low temperature fields in Southern Bulgaria. In: Report 7 for the UN Geothermal Train. Program. National Energy Authority, Reykjavik, Iceland (40 pp.).

Hristov, V., Benderev, A., Bojadgieva, K., 2010. Assessment of hydrogeological and hydrochemical conditions in Kazanlak basin (Bulgaria). In: Proc. 2010 World Geothermal Congress, 25–30 Apr., Bali, Indonesia.

Ingebritsen, S.E., Sanford, W.E., Neuzil, C.E., 2006. Groundwater Flow in Geologic Processes, 2nd ed. Cambridge Univ. Press, Cambridge, UK. (536 pp).

Javoy, M., Pineau, F., Demaiffe, D., 1984. Nitrogen and carbon isotopic composition in the diamonds of Mbuji Mayi (Zaire). Earth Planet. Sci. Lett. 68, 399–411.

Jenden, P.D., Kaplan, I.R., Poreda, R.J., Craig, H., 1988. Origin of nitrogen-rich natural gases in the California Great Valley: evidence from helium, carbon and nitrogen isotope ratios. Geochim. Cosmochim. Acta 52, 851–861.

Kaiser-Rohrmeier, M., Handler, R., v. Quadt, A., Heinrich, C., 2004. Hydrothermal Pb–Zn ore formation in the Central RhodopianDome, south Bulgaria: Review and new time constraintsfrom Ar–Ar geochronology. Schweizerische Mineralogische und Petrographische Mitteilungen 84, 37–58.

Karydakis, G., Arvanitis, A., Andritsos, N., Fytikas, M., 2005. Low enthalpy geothermal fields in the Strymon basin (Northern Greece). In: Proc. 2005 World Geothermal Congress, 24–29 April, Antalya, Turkey, (Paper No. 2615) (12 pp).

Karytsas, C., 1990. Inventory of low enthalpy geothermal resources discovered through deep oil and gas exploration wells. In: Centre for Renewable Energy Sources, Internal Rep. for Contract DG XVII 7030/ETD/89-6, Pikermi, Greece (150 pp).

Katsoyiannis, I.A., Katsoyiannis, A.A., 2016. Arsenic and other metal contamination of groundwaters in the industrial area of Thessaloniki, Northern Greece. Environ. Monit. Assess. 123, 393–406.

Kojumdgieva, E., Stojkov, S., Markova, S., 1984. Lithostratigraphy of the Neogene sediments in the Toundza Basin. Spisanie na Bălgarskoto Geologičesko Družestvo 45, 287–295 (in Bulgarian).

Koriting, S., 1974. Fluorine. In: Wedephol, K.H. (Ed.), Handbook of Geochemistry, 1: Chapter 9-D. Springer Verlag, Berlin, pp. 1–11.

Kounov, A., Seward, D., Burg, J.-P., Bernoulli, D., Ivanov, Z., Handler, R., 2010. Geochronological and structural constraints on the Cretaceous thermotectonic evolution of the Kraishte zone, western Bulgaria. Tectonics 29. https://doi.org/10.1029/2009TC002509.

Kounov, A., Graf, J., von Quadt, A., Bernoulli, D., Burg, J.-P., Seward, D., Ivanov, Z., Fanning, M., 2012. Evidence for a "Cadomian" ophiolite and magmatic-arc complex in SW Bulgaria. Precambrian Res. 212-213, 295. https://doi.org/10.1016/j.precamres.2012.06.003.

Kounov, A., Wütrich, E., Seward, D., Burg, J.-P., Stockli, D., 2015. Low-temperature constraints on the Cenozoic thermal evolution of the Southern Rhodope Core Complex (Northern Greece). Intl. J. Earth Sci. 104, 1337–1352.

Krohe, A., Mposkos, E., 2001. Structural evolution and exhumation history of the Rhodope UHP-HP metamorphic province (Northern Greece). Bull. Geol. Soc. Greece 34, 75–82.

Langelier, W.F., Ludwig, H.F., 1942. Graphical method for indicating the mineral character of natural waters. J. Am. Water-works Ass. 34, 335–352.
Li Vigni, L., Daskalopoulou, K., Calabrese, S., Kyriakopolous, K., Parello, F., Brugnone, F., D'Alessandro, W., 2021. Geochemical characterisation of the thermo-mineral waters of Greece. Environ. Geochem. Health. https://doi.org/10.1007/s10653-021-01001-1.
Longinelli, A., Selmo, E., 2003. Isotopic composition of precipitations in Italy: a first overall map. J. Hydrol. 270, 75–88.
Lowenstern, J.B., Bergfeld, D., Evans, W.C., Hunt, A.G., 2015. Origin of geothermal gases at Yellowstone. J. Volcanol. Geothermal Res. 302, 87–101.
Magro, G., Pennisi, M., 1991. Noble gases and nitrogen: mixing and temporal evolution in the fumarolic fluids of Vulcano, Italy. J. Volcanol. Geothermal Res. 47, 237–247.
Magro, G., Gherardi, F., Bellani, S., 2010. Noble gases in karstic and thermal waters of Strymon basin (Greece-Bulgaria). In: 13th Intl. Symp on Water-Rock Interac., Birkle P., Torres Alvarado I.S. eds, 16–20 Aug., Guanajuato (Mexico), pp. 345–348.
Marty, B., Jambon, A., 1987. $C/^3He$ in volatile fluxes from the solid earth: implications for carbon geodynamics. Earth Planet. Sci. Lett. 83, 16–26.
Meinhold, G., Kostopoulos, D., Frei, D., Himmerkus, F., Reischmann, T., 2010. U-Pb LA-SF-ICP-MS zircon geochronology of the Serbo-Macedonian Massif: paleotectonic constraints for Gondwana-derived terrains in the Easter Mediterranean. Intern. J. of Earth Sci. 99, 813–832.
Mendrinos, D., Choropanitis, I., Polyzou, O., Karytsas, C., 2010. Exploring for geothermal resources in Greece. Geothermics 39, 124–137.
Minissale, A., 2004. Origin, transport and discharge of CO_2 in central Italy. Earth Sci. Rev. 66, 89–141.
Minissale, A., 2018. A simple geochemical prospecting method for geothermal resources in flat areas. Geothermics 72, 258–267.
Minissale, A., Vaselli, O., 2011. Karst springs as "natural" pluviometers: constraints on the isotopic composition of rainfall in the Apennines of Central Italy. Appl. Geochem. 26, 838–852.
Minissale, A., Duchi, V., Kolios, N., Totaro, G., 1989. Geochemical characteristics of Greek thermal springs. J. Volcanol. Geotherm. Res. 39, 1–16.
Minissale, A., Vaselli, O., Chandrasekharam, D., Magro, G., Tassi, F., Casiglia, A., 2000. Origin and evolution of "intracratonic" thermal fluids from central-western peninsular India. Earth Planet. Sci. Lett. 181, 377–394.
Montegrossi, G., Tassi, F., Vaselli, O., Buccianti, A., Garofalo, K., 2001. Sulfur species in volcanic gases. Anal. Chem. 73, 3709–3715.
Morland, G., Reimann, C., Strand, T., Skarphaugen, H., Banks, D., Bjorvatn, K., Hall, G.E. M., Siewers, U., 1997. The hydrogeochemistry of Norwegian bedrock groundwater-selected parameters (pH, F^-, Rn, U, Th, B, Na, Ca) in samples from Vestfold and Hordaland, Norway. Norges Geol. Undersøk. Bull. 432, 103–317.
Mountrakis, D., Tranos, M., Papazachos, C., Thomaidou, E., Karagianni, E., Vamvakaris, D., 2006. New neotectonic and seismological data about the main active faults and stress regime of Northern Greece. J. Geol. Society, London, Spec. Public. 260, 649–670.
Mouslopoulou, V., Saltogianni, V., Gianniou, M., Stiros, S., 2014. Geodetic evidence for tectonic activity on the Strymon Fault System, northeast Greece. Tectonophysics 633, 246–255.
Nisi, B., Vaselli, O., Marchev, P., Tassi, F., 2013. Diffuse CO_2 soil flux measurements at the youngest volcanic system in Bulgaria: the 12.2 Ma old Kozhuh cryptodome. Acta Vulcanol. 25, 169–178.
Oliver, J., 1986. Fluids expelled tectonically from orogenic belts: their role in hydrocarbon migration and other geologic phenomena. Geology 14, 99–102.
O'Nions, R.K., Oxburgh, E.R., 1988. Helium volatile fluxes and the development of continental crust. Earth Planet. Sci. Lett. 90, 331–347.
Parkhurst, D.L., Appelo, C.A.J., 1999. User's guide to PHREEQC (Version 2)-a computer program for speciation, batch-reaction, one-dimensional transport, and inverse geochemical calculations. U.S. Geological Survey, WRIR 312, 99–4259.
Pentcheva, E., Van't dack, L., Veldeman, E., Hristov, V., Gijbels, R., 1997. Hydrogeochemical Characteristics of Geothermal Systems in South Bulgaria. Universiteit Antwerpen (UIA), Belgium.
Petrov, P.S., 1964. Basic regularities in mineral waters distribution in Bulgaria. In: Proc. of Geology of Bulgaria, Series Engin. Geol. Hydrogeol, vol. 3, pp. 83–158.
Petrov P.S. (1973) Map of mineral waters in PR Bulgaria at scale 1:1,000,000. Atlas of PR Bulgaria.
Petrov, P., Martinov, S., Limonadov, K., Straka, Y., 1970. Hydrogeological Investigations of Mineral Waters in Bulgaria. PH Technika, p. 196.
Philippon, M., Brun, J.P., Gueydan, F., Sokoutis, D., 2014. The interaction between Aegean back-ark extension and Anatolia escape since Middle Miocene. Tectonophys. 631, 176–188.
Piperov, N.B., Kamensky, I.L., Tolstikhin, I.N., 1994. Isotopes of light noble gases in mineral waters in the eastern part of the Balkan peninsula, Bulgaria. Geochim. Cosmochim. Acta 58, 1889–1898.
Quolin, S., Van Den Broek, M., Declaye, S., Dewallef, P., Lemort, V., 2013. Techno-economic survey of Organic Rankine cycle (ORC) system. Sust. Energy Rev. 22, 168–186.
Radev, N., 1930. Mineral waters: brief geological and historical review. Review of the Balneological Association, Bulgaria vol. 1, 1–5 (in Bulgarian).
Ricou, L.-E., Burg, J.-P., Godfriaux, I., 1998. Rhopode and Vardar: The metamorphic and the olistostromic paired belts to the Cretaceous subduction under Europe. Geodinamica Acta 11, 285–309.
Sano, Y., Fischer, T.P., 2013. The analysis and interpretation of noble gases in modern hydrothermal systems. In: Burnard, P. (Ed.), The Noble Gases as Geochemical Tracers, Advances in Isotope Geochemistry. Springer, Berlin, Heidelberg, pp. 249–317.
Sano, Y., Marty, B., 1995. Origin of carbon in fumarolic gas from island arcs. Chem. Geol. Isot. Geosci. 119, 265–274.
Shterev, K., Penev, I., 1991. Overview of geothermal resources and activities in Bulgaria. Geothermics 20, 91–98.
Shterev, K., Zagortchev, I., Shterev, D., 1995. Geothermal resources and systems in the Strymon rift valley (Bulgaria and Greece). In: Proc. 1995 Geothermal Congress, 18–31 May, Florence, Italy, vol. 2, pp. 1185–1191.
Skoulikidis, N.T., Zogaris, S., Economou, N., Gritzalis, C., 2009. Rivers of the Balkans. In: Tockner, K., Uehlinger, U., Robinson, C. (Eds.), Rivers of Europe. Academic Press, pp. 421–466.
Smedley, P.L., Kinniburgh, D.G., 2017. Molybdenum in natural waters: a review of occurrence, distributions and controls. Appl. Geochem. 84, 387–432.
Tassi, F., Vaselli, O., Tedesco, D., Montegrossi, G., Darrah, T., Cuoco, E., Mapendano, M. Y., Poreda, R., Delgado, Huertas A., 2009. Water and gas chemistry at Lake Kivu (DRC): geochemical evidence of vertical and horizontal heterogeneities in a multi-basin structure. Geochem. Geophys. Geosyst. 10 (2) https://doi.org/10.1029/2008GC002191.
Tassi, F., Fazi, S., Rossetti, S., Pratesi, P., Ceccotti, M., Cabassi, J., Capecchiacci, F., Venturi, S., Vaselli, O., 2018. The biogeochemical vertical structure renders a meromictic volcanic lake a trap for geogenic CO_2 (Lake Averno, Italy). PLoS One 13 (3), e0193914. https://doi.org/10.1371/journal.pone.0193914.
Towler, B.F., 2014. Chapter 11-geothermal energy. In: Towler, B.F. (Ed.), The Future of Energy. Elsevier (390 pp.).
Tranos, M.D., 2011. Strymon and Strymonikos Gulf basins (Northern Greece): implications on their formation and evolution from faulting. J. Geodynamics 51, 285–305.
Turpaud, P., Reischmann, T., 2010. Characterization of igneous terrains by zircon dating: implications for UHP occurrences and suture identification in the central Rhodope, northern Greece. Intern. J. Earth Sci. 99, 567–591.
Vaselli, O., Tassi, F., Montegrossi, G., Capaccioni, B., Giannini, L., 2006. Sampling and analysis of volcanic gases. Acta Volcanol. 18, 65–76.
Velinov, T., Bojadgieva, K., 1981. Geothermal Investigations in Bulgaria. PH Technika, p. 154 (in Bulgarian).
Venturi, S., Tassi, F., Bicocchi, G., Cabassi, J., Capecchiacci, F., Capasso, G., Vaselli, O., Ricci, A., Grassa, F., 2018. Fractionation processes affecting the stable carbon isotope signature of thermal waters from hydrothermal/volcanic systems: the examples of Campi Flegrei and Vulcano Island (southern Italy). J. Volcanol. Geotherm. Res. 345, 46–57.
Venturi, S., Tassi, F., Magi, F., Cabassi, J., Ricci, A., Capecchiacci, F., Caponi, C., Nisi, B., Vaselli, O., 2019. Carbon isotopic signature of interstitial soil gases reveals the potential role of ecosystems in mitigating geogenic greenhouse gas emissions: Case studies from hydrothermal systems in Italy. Sci. Total Environ. 655, 887–898.
Vrablyanski, B., Milev, G., 1993. Neotectonic features of the Struma fault zone. Acta Montana IGt Ass. Cr. Series A 4, 111–132.
Wilhelm, E., Battino, R., Wilcock, R.J., 1977. Low-pressure solubility of gases in liquid waters. Chem. Rev. 77, 219–230.
Zagorchev, I., 1992. Neotectonic development of the Struma (Kraištid) Lineament, southwest Bulgaria and northern Greece. Geol. Mag. 129, 197–222.
Zagorchev, I., 2007. Late Cenozoic development of the Strouma and Mesta fluviolacustrine systems, SW Bulgaria and northern Greece. Quatern. Sci. Rev. 26, 2783–2800.